Drosophila with-no-lysine and *frayed* Act in Parallel to dSarm to Drive Neurodegeneration Following dNmnat Depletion

Adel Avetisyan[1], Romina Barria[1], Amy Sheehan[1], Marc R. Freeman[1,2]

[1] Vollum Institute, Oregon Health and Science University, Portland, OR 97239

[2] Lead contact

Summary

The maintenance of neuronal circuits is vital for sustaining nervous system function throughout life. Neurons are particularly susceptible to damage from metabolic and environmental stressors, which can lead to various neurodegenerative diseases. Over the past three decades, research has identified critical neuronal survival factors like Nmnat2 and key drivers of axon destruction, such as Sarm1, following neuronal injury. Further research has highlighted Sarm1's essential role in neurodegeneration; however, much remains unknown about its activation, mechanisms of action, and potential interacting pathways that mediate neurodegeneration.

To explore these questions, we used *Drosophila*, a model system that previously enabled us to identify mutations in pro-degenerative genes such as *dSarm* following injury. We developed a novel method to trigger degeneration via neuron-intrinsic dNmnat depletion—a conserved approach for inducing dSarm-dependent degeneration. Conducting a forward genetic screen of nearly 5,000 chromosomes, we identified several protective mutations, including two loss-of-function alleles of the *Drosophila with-no-lysine* (*dWnk*) gene, which encodes a conserved serine/threonine kinase uniquely sensitive to intracellular chloride and potassium levels. Our findings reveal that dWnk, along with its downstream kinase Frayed (Fray; ortholog of mammalian OSR1/SPAK), promotes neurodegeneration caused by dNmnat depletion and that kinase activities of both proteins are essential to this signaling event. We found that dWnk is activated in parallel with dSarm to drive neurodegeneration following dNmnat depletion. Furthermore, simultaneous inhibition of both dSarm- and dWnk-mediated pathways provides neurons with near-complete protection from dNmnat depletion. Interestingly, activation of the dWnk pathway reduces the neuroprotection afforded by a *dSarm* null allele following dNmnat depletion but not axonal injury. This distinction highlights mechanistic differences between dNmnat depletion and other injury models and suggests that dWnk/Fray signaling may rely on the presence of the neuronal cell body. Overall, our innovative screening approach revealed pathways driving neurodegeneration in parallel to Sarm1 and indicates that targeting these pathways alongside Sarm1 inhibition could enhance therapeutic strategies against neurodegeneration.

Introduction

Maintenance of neuronal integrity is essential for sustained nervous system function across lifespan. As highly metabolically active cells, neurons are particularly vulnerable to a variety of insults, including metabolic disorders, mitochondrial dysfunction, toxin exposure, and physical injury. These vulnerabilities can lead to neurodegeneration and the loss of neuronal connectivity, hallmark features of neurological disorders such as Alzheimer's and Parkinson's diseases (Kasahara et al., 2010; Burke and O'Malley, 2013; Kneynsberg et al., 2017; Coleman and Höke, 2020), but how neurodegeneration is triggered in any context remains poorly understood (Coleman and Höke, 2020).

Axotomy has served as a useful approach to characterize signaling molecules required for axon degeneration. Studies beginning with the *Wallerian degeneration slow* (*Wld*^{S}) molecule (Lunn et al., 1989) and the NAD^+ biosynthetic enzyme NMNAT2 revealed that axonal survival is critically dependent on the delivery of NMNAT2 from the cell body to the axon (Gilley and Coleman, 2010; Milde et al., 2013). After axotomy, the labile NMNAT2 molecule is degraded (Wang et al., 2005), its substrate NMN accumulates. This accumulation then activates SARM1 (*sterile alpha/Armadillo/Toll-Interleukin receptor (TIR) homology domain protein*) (Di Stefano et al., 2015; Zhao et al., 2019; Bratkowski et al., 2020; Figley et al., 2021) to deplete pools of NAD^+ though a hydrolase activity intrinsic to its TIR domain (Gerdts et al., 2015; Essuman et al., 2017) and drive axon degeneration. Remarkably, while *NMNAT2* null mutants die perinatally with short axons, *NMNAT2, SARM1* double mutants survive and appear phenotypically normal, arguing that a significant part of pro-degenerative signaling that occurs after NMNAT2 loss flows through SARM1 (Gilley et al., 2015). SARM1 is believed to act as a metabolic sensor after depletion of NMNAT2. In healthy cells, NAD^+ binding to the ARM domain of SARM1 stabilizes interactions between its ARM-TIR domains and inhibits hydrolase activity (Sporny et al., 2020; Figley et al., 2021), while binding of the NMN that accumulates after NMNAT2 depletion destabilizes ARM-TIR association and promotes activation (Zhao et al., 2019; Bratkowski et al., 2020; Figley et al., 2021). Interestingly, although initially identified as required for axotomy, SARM1 and NMNAT2 signaling appear to be deployed broadly across the nervous system and used to drive neurodegeneration in a wide variety of contexts including retinal degeneration (Sasaki et al., 2020), peripheral neuropathies (Geisler et al., 2016, 2019; Turkiew et al., 2017; Sato-Yamada et al., 2022) and traumatic brain injury (Henninger et al., 2016; Marion et al., 2019; Bradshaw et al., 2021). Intriguingly, genome-wide association studies recently identified mutations in the ARM domain of hSARM1 that render it constitutively active in ALS patients, positioning SARM1 locus as a risk factor for ALS development (Gilley et al., 2021; Bloom et al., 2022).

Additional mechanisms that lead to the activation of SARM1 signaling remain poorly defined, as do signaling events downstream of SARM1. In *Drosophila*, dSarm activation promotes neurodegeneration through a BTB and C-terminal Kelch (BACK) domain protein Axundead (Axed). Loss of Axed is sufficient to completely block the degenerative effects of dSarm activation (Neukomm et al., 2017) and *dSarm* and *axed* mutants are capable of suppressing neurodegeneration induced by depletion of *Drosophila* Nmnat (dNmnat) by RNAi, indicating that depletion of NMNAT molecules is a conserved mechanism for SARM1/dSarm activation. While mammals have three NMNAT isoforms—nuclear NMNAT1, cytoplasmic NMNAT2 and mitochondrial NMNAT3—there is only one dNmnat molecule in the fly genome. Surprisingly, while *dSarm* mutants can suppress neurodegeneration induced by partial depletion of dNmnat, *dSarm* null mutants cannot rescue *dNmnat* null mutant clones while *axed* mutants can (Neukomm et al., 2017). This observation indicates the loss of Axed is even more neuroprotective than loss of dSarm and that additional signaling mechanisms must exist that flow into Axed to drive neurodegeneration (Neukomm et al., 2017).

To identify additional regulators of neuronal NAD^+ pathways and dSarm/SARM1-related neurodegeneration, we conducted an unbiased forward genetic screen using a novel method of dNmnat depletion to activate dSarm-dependent neurodegeneration (Gilley and Coleman, 2010; Neukomm et al., 2017). We identified the *Drosophila with-no-lysine* (*dWnk*) gene, which encodes a conserved serine/threonine kinase (Goldsmith and Rodan, 2023). Unlike typical kinases, WNK proteins have their catalytic lysine located in sub-domain I (Xu et al., 2000; Veríssimo and Jordan, 2001), enabling them to sense chloride and potassium levels within a cell (Piala et al., 2014;

Pleinis et al., 2021). The WNK pathway's most studied function is the regulation of Na^+ absorption and K^+ secretion in the kidneys. Gain-of-function mutations in WNK1/4 and loss-of-function mutations in proteins regulating their abundance cause Familial Hyperkalemic Hypertension (FHHt) syndrome (Wilson et al., 2001; McCormick et al., 2008). WNKs are activated by auto-phosphorylation and signal through downstream Ser/Thr kinases SPAK (STE20/SPS1-related, proline alanine-rich kinase) and OSR1 (Oxidative-stress responsive 1)(*Drosophila* Frayed), driving intracellular Cl^- accumulation by phosphorylating NKCC1/2 ($Na^+/K^+/2Cl^-$)/ NCC (Na^+/Cl^-) to promote Cl^- influx and KCC1-4 (K^+/Cl^-) to prevent Cl^- efflux (Dowd and Forbush, 2003; Moriguchi et al., 2005; Vitari et al., 2005; Anselmo et al., 2006; Ponce-Coria et al., 2008; Richardson et al., 2008; Sengupta et al., 2012). Mutations in the HSN2 exon of WNK1, which is spliced in only in the nervous system, lead to hereditary neuropathy HSANII (Lafrenière et al., 2004; Rivière et al., 2004; Shekarabi et al., 2008), and WNKs/SPAK/OSR1/NKCC1 are known to be activated under pathological conditions such as stroke (Bhuiyan et al., 2020). Curiously, a recent study also revealed an interesting genetic link between dWnk, dSarm and Axundead in *Drosophila*, where loss of dWnk led to dSarm/Axed-dependent developmental phenotypes and distal axon retraction (Izadifar et al., 2021). Here we show, in contrast, that dNmnat depletion induces neurodegeneration that requires dWnk and Fray, and that this pathway signals in parallel with dSarm to drive neurodegeneration through Axed. Our work identifies the dWnk pathway as a key signaling partner for dSarm, which is required for maximal activation of neurodegeneration after depletion of dNmnat.

Results

Drosophila With-no-lysine kinase (dWnk) promotes neurodegeneration induced by dNmnat depletion

Glutamatergic sensory neurons located in the L1 nerve of the *Drosophila* anterior wing vein extend their axons medially into the thoracic CNS (Fang et al., 2012; Neukomm et al., 2014). We used Mosaic Analysis with a Repressible Cell Marker (MARCM) to simultaneously label single-cell clones with membrane-tethered GFP while inducing neurodegeneration by depleting dNmnat using a *UAS-RNAi* construct (Fig. S1A) (Wu and Luo, 2006). In control MARCM clones (no RNAi), the vast majority of glutamatergic sensory neuron cell bodies, dendrites, and axons remained intact for the lifespan of the fly. However, when we drove a *UAS-dNmnat*^{RNAi} construct in MARCM clones generated on the left arm of chromosome 3, we found that the majority of axons and dendrites showed signs of fragmentation by days 3-5 after animals eclosed as adults and cell bodies shrunk. By 10 days after eclosion, >85% axons and dendrites were cleared along with most neuronal cell corpses, although cell corpses seemed to be eliminated later than neurites (Fig 1B-D).

To identify new molecules that drive neurodegeneration after dNmnat depletion, we performed an unbiased EMS-based forward genetic screen for mutations that cell-autonomously suppressed neurodegeneration in the presence of dNmnat^{RNAi}. In total, we screened 4,917 mutagenized chromosomes on the left arm of chromosome 3 in MARCM clones for suppression of dNmnat^{RNAi}-induced neurodegeneration. Among several candidate mutations, we identified two lines, *3L.282* and *3L.1541*, which resulted in strong suppression of neurodegeneration, with 57.9% and 63.9% of neurons remaining intact, respectively, compared to 18.6% in controls (Fig. 1B, C). We noted that cell bodies in these lines were slightly more protected than axons (Fig. 1D), suggesting that axonal degeneration might be an earlier event after loss of dNmnat.

Complementation crosses revealed that lines *3L.282* and *3L.1541* failed to complement each other, and both failed to complement two molecularly defined genomic deletions, *Df(3L)ED4978* (Ryder et al., 2007) and *Df(3L)Exel9066. Df(3L)ED4978* spans 346.9 kb, while *Df(3L)Exel9066* only spans 14.9 kb, and both delete the *Drosophila with-no-lysine kinase* (*dWnk*) locus along with two neighboring genes (Fig. S1B, S1C). Whole genome sequencing (WGS) of the *3L.282* line revealed a C-to-T mutation in *dWnk* that alters a splice donor site in intron nine, affecting all four *dWnk* transcripts (Fig. S1B, D). However, sequencing of *3L.1541* did not reveal any mutations in the *dWnk* coding region, suggesting this mutation could affect a regulatory region of *dWnk* (Fig. S1D).

To confirm that loss of dWnk caused the suppression of neurodegeneration after *dNmnat* knockdown in these mutant lines, we assayed two available null alleles of *dWnk* in MARCM clones, *Df(3L)Exel9066* and $dWnk^{MB06499}$ (Serysheva et al., 2013)(Fig. 1A and S1B, D). We found they both exhibited similar preservation of axons and cell bodies when compared to mutants *3L.282* and *3L.1541* (Fig. 1B-D). In addition, reintroducing wild-type *dWnk* ($UAS\text{-}dWnk^{WT}$) into MARCM clones in these backgrounds restored neurodegeneration upon dNmnat depletion (Fig. 1B-D, and S1F). These data indicate that *3L.282* and *3L.1541* are loss-of-function mutations in *dWnk*, and that dWnk is required to drive neurodegeneration after dNmnat loss. In summary, our data reveals a pro-degenerative role for dWnk in neurodegeneration that is activated by cell-autonomous depletion of dNmnat.

A previous study reported that other loss-of-function alleles, $dWnk^{F1183}$ and $dWnk^{G1286}$ (Fig. S1D), resulted in opposite effects, with highly branched pSC and pDC mechanosensory neurons in these mutant backgrounds showing defects in axon pathfinding and maintenance that could be suppressed by mutation of *dSarm* or *axundead* (Izadifar et al., 2021). Surprisingly, the above *dWnk* alleles did not protect against neurodegeneration induced by *dNmnat* depletion in our hands (Fig. S1G), suggesting they might be weaker, partial loss-of-function alleles – rather than nulls – given the uniform protection we found using the molecularly defined null alleles above. To investigate whether knocking out dWnk led to spontaneous degeneration in either the glutamatergic L1 wing sensory neurons we studied or an orthogonal set of neurons, the cholinergic $OR22a^{+}$ olfactory receptor neurons, we analyzed homozygous neuronal clones of various *dWnk* alleles in these cell types, including $dWnk^{F1183}$ and $dWnk^{G1286}$, and found they remained morphologically intact late into adulthood (Fig. S1H). This discrepancy in functional roles for dWnk in cell maintenance and activation of dSarm-sensitive degenerative event could point to a cell-specific role for dWnk in pSC and pDC for their development and maintenance (see also Discussion).

dWnk kinase activity is required for pro-degenerative signaling

dWnk, like mammalian WNKs (WNK1-4), is a kinase that acts as sensor for ions such as chloride and potassium and can also be activated by changes in osmotic pressure (Fig. 1A)(Goldsmith and Rodan, 2023; Yarikipati et al., 2023). We sought to determine which of these functions might regulate dWnk signaling in the context of neurodegeneration after dNmnat depletion. To determine whether the kinase and Cl^{-} binding activities of dWnk are required for its pro-degenerative role after dNmnat loss, we used a number of UAS- transgenes with modified forms of dWnk: an S632A mutation that disrupts auto-activation of dWnk via phosphorylation (Xu et al., 2002; Zagórska et al., 2007), a D618A mutation that generates a dominant-negative dWnk lacking kinase activity (Sato and Shibuya, 2013; Serysheva et al., 2013; Wu et al., 2014), and an L619F mutation that reduces dWnk's Cl^{-} sensitivity, rendering it constitutively active (Piala et al., 2014)

(Fig. 2A). We first expressed these in wild type clones and found that constitutive expression of *dWnk*^{S632A} or *dWnk*^{L619F} did not affect the survival of wild type clones, however expression of *dWnk*^{D618A} did result in a slight reduction in cell survival (Fig. S2A). We next generated dNmnat^{RNAi}-expressing MARCM clones and expressed each transgene and assayed for suppression of neurodegeneration. We found that expression of *dWnk*^{S632A} did not suppress neurodegeneration after dNmnat depletion, suggesting that dWnk auto-activation by phosphorylation is not crucial for its pro-degenerative role (Fig. 2B and S2B). In contrast, expression of the dominant-negative *dWnk*^{D618A} molecule strongly suppressed neurodegeneration in the dNmnat^{RNAi} background, providing additional evidence for a pro-degenerative role for dWnk after dNmnat depletion (Fig. 2B and S2B). Finally, expression of the constitutively activated, Cl^--insensitive *dWnk*^{L619F} molecule did not suppress neurodegeneration after dNmnat loss (Fig. 2B and S2B).

We next tested whether each of these dWnk variants could rescue the *dWnk*$^{3L.282}$ mutant's suppression of neurodegeneration after dNmant knockdown. We found that expression of *dWnk*^{S632A} or *dWnk*^{L619F} were sufficient to rescue *dWnk*$^{3L.282}$ mutant phenotypes, while expression of the dominant negative *dWnk*^{D618A} molecule was not (Fig. 2C, D and S2C-E). We observed similar phenotypes when we examined the survival of neuronal cell bodies (Fig. S2C, E), and in the *Df(3L)Exel9066* and *dWnk*^{MB06499} backgrounds with *dWnk*^{S632A} (Fig. S2F, G). Together, these data argue the auto-activation by phosphorylation and Cl^- sensing functions of dWnk are not required for pro-degenerative signaling while dWnk kinase activity is essential, and that activation of dWnk signaling only drives neurodegeneration after depletion of dNmnat and not in wild type neurons.

Fray acts downstream of dWnk to promote neurodegeneration

Mammalian WNK kinases signal through downstream kinases SPAK/OSR1, which in *Drosophila* is encoded by the *frayed* (*fray*) gene (Leiserson et al., 2000) (Fig. 3A). WNKs phosphorylate SPAK/OSR1/Fray at specific sites that lead to the activation of downstream cation-chloride co-transporters (Moriguchi et al., 2005; Vitari et al., 2005; Anselmo et al., 2006; Sato and Shibuya, 2013; Wu et al., 2014; Schellinger et al., 2022) (Fig. 3A, B). We therefore sought to determine whether dWnk signals through Fray to drive neurodegeneration after dNmnat loss. The *fray* gene overlaps with *CG7694* (Fig. S3A), and we used the P-element insertion loss-of-function allele for *fray*, *fray*^{07551} (Russell et al., 1998; Spradling et al., 1999). When we crossed *fray*^{07551} into a dNmnat^{RNAI} background, we observed strong neuroprotection, with ~60% of neurons surviving in homozygous mutant MARCM clones (Fig. 3C, E, F). We confirmed this phenotype by generating two additional alleles of *fray*: a deletion allele (*fray*$^{\Delta}$), and a genome engineered version that eliminated the catalytic lysine at position 67 (*fray*^{K67M}). We found that, while the *fray*$^{\Delta}$ allele suppressed neurodegeneration activated by dNmnat depletion in MARCM clones, the kinase-impaired allele *fray*^{K67M} (Sato and Shibuya, 2013) demonstrated slightly reduced neuroprotection compared to the null allele (Fig. 3D), confirming a role for Fray and likely its kinase activity in pro-degenerative signaling.

Fray has two key phosphorylation sites that drive activation, S347 and T206. We used the phospho-mimicking Fray^{S347D} and Fray^{T206E} versions of these, along with the kinase impaired Fray^{D185A} version, to explore how Fray signaling drive neurodegeneration. We expressed each of these in *fray*^{07551} MARCM clones expressing dNmnat^{RNAi} and found that both Fray^{S347D} and Fray^{T206E} promoted rapid neurodegeneration while expression of Fray^{D185A} did not (Fig. 3C, E, F). Expression of each of these constructs in wild type MARCM clones in neurons did not result in

neurodegeneration (Fig. S3B), suggesting that activation of Fray alone is insufficient to induce neurodegeneration and rather that it only can promote neurodegeneration after dNmant loss.

To determine whether Fray functions downstream of dWnk during neurodegeneration, we expressed an activated form of Fray (Fray^{S347D}) in *dWnk* loss-of-function mutant backgrounds. As expected, we found Fray^{S347D} was sufficient to overcome the protective effects of *dWnk*$^{3L.282}$ and *dWnk*^{MB06499}, while the kinase impaired Fray^{D185A} was not (Fig. 3G, H and S3C-F). In contrast, expression of the activated form of dWnk (dWnk^{L619F} (Piala et al., 2014)) in a *fray*^{07551} background did not diminish the neuroprotection afforded by the *fray* mutant (Fig. 3C, E, F). In all cases, we observed similar phenotypes in axons and cell bodies in MARCM clones (Fig. 3E, F- H and S3C-F), suggesting that axons and cell bodies use dWnk and Fray signaling similarly to drive axon degeneration and cell death. In summary, these data support a model whereby dWnk activation signals downstream to Fray to drive neurodegeneration induced by dNmnat loss.

dWnk Acts in Parallel to dSarm to drive neurodegeneration

Our previous work demonstrated Axundead (Axed) functions downstream of dSarm in Wallerian degeneration (Neukomm et al., 2017). Impressively, loss of *axed* confers near-complete protection across various neurodegenerative paradigms, including axotomy or even null alleles of *dNmnat* (Neukomm et al., 2017). In contrast, while *dSarm* nulls protect axons at similar levels after axotomy, *dSarm* nulls only partially protect against *dNmant* knockdown and fail to suppress neurodegeneration induced by *dNmnat* null mutations(Neukomm et al., 2017). To explore the relationship between dSarm, Axed, and the dWnk/Fray pathway, we utilized the temperature-sensitive *UAS/Gal4* expression system to induce partial knockdown of *dNmnat*. We conducted experiments at 29°C to increase *UAS-dNmnat*^{RNAi} expression, resulting in more rapid neurodegeneration than at 25°C as in previous experiments. In this context, 95% of *UAS-dNmnat*^{RNAi}-expressing wild type MARCM clones degenerated by 8 dpe (Fig. 4A-C) compared to approximately 70% by 10 dpe at 25°C (Fig. S4A, B). Similarly, while at 25°C we observed 70% protection by a *dSarm* null allele (*dSarm*^{896} (Osterloh et al., 2012)) (Fig. S4A, B), at 29°C protection decreased to 46-50% (Fig. 4A-C) and *dWnk* null mutant neuroprotection decreased from 57-60% at 25°C (Fig. S4A, B) to 31-38% at 29°C (Fig. 4A-C). Interestingly, when we assayed genetic null alleles of *dSarm, dWnk* double mutants (*dSarm*^{896}, *dWnk*$^{3L.282}$), we found an additivity of protection, with 85% *dSarm*^{896}, *dWnk*$^{3L.282}$ MARCM clones remaining intact (Fig. 4A-C). We found similar results using another double mutant combination, *dSarm*^{896}*, dWnk*^{MB06499} (Fig. S4C, D), and this was true in both axons and cell bodies (Fig 4B, C and 4SA-D). Given our use of null alleles, the additive nature of this phenotype argues that dWnk and dSarm act in parallel to drive neurodegeneration in the context of dNmnat depletion (Fig. 5B). Finally, we found that the additivity in *dSarm*, *dWnk* double mutants was equivalent to null mutations in *axed* (*axed*$^{3L.11}$ (Neukomm et al., 2017)) (Fig 4B,C and S4A-D).

Can activation of dSarm or dWnk/Fray signaling bypass protection conferred by inhibiting the other? To test this possibility, we first expressed a gain-of-function form of dSarm that lacks the auto-inhibitory ARM domain (Chuang, 2005; Neukomm et al., 2017) (*dSarm*$^{\Delta ARM}$). This resulted in rapid neurodegeneration that was unaffected by either *dWnk* or *fray* null mutations (Fig. 4D). In contrast, while expression of the activated version of dWnk (dWnk^{L619F}) or Fray (Fray^{S347D}) did not trigger spontaneous neurodegeneration at 29°C on their own in control MARCM clones (Fig. 4I), expression of either in *UAS-dNmnat*^{RNAi} neurons significantly reduced the protection offered by *dSarm*^{896} (Fig. 4E-H). Finally, we note that expressing kinase-impaired forms of either dWnk or Fray could not override *dSarm* null background protection (Fig. 4E-H). These data support a

model whereby dWnk and Fray act in parallel, with activation of either pathway being sufficient to overcome the other in the context of neurodegeneration after dNmant loss (Fig. 5B).

dWnk/Fray and dSarm converge on Axed to drive neurodegeneration

To determine whether dWnk and Fray signal via Axed, we expressed an activated version of Fray ($Fray^{S347D}$) in an *axed* null mutant background expressing $dNmant^{RNAi}$. Interestingly, although expression of $Fray^{S347D}$ was sufficient to overcome the protection afforded by *dSarm* nulls, activated Fray was not sufficient to overcome the strong protection afforded by *axed* mutants (Fig. 5A). This observation, coupled with the additivity of *dSarm* and *dWnk/Fray* null mutants, supports a model whereby, after depletion of dNmnat, dSarm and dWnk/Fray act in parallel to drive neurodegeneration through Axed (Fig. 5B).

dWnk/Fray may signal through the cell body to promote neurodegeneration

Although mutations in *dWnk* and *fray* can suppress neurodegeneration that is activated by dNmnat depletion, we found *dWnk* mutations did not block axon degeneration after axotomy (Fig. 5C). We next explored the possibility that *dWnk* mutations might enhance *dSarm* mutant phenotypes after axotomy. In previous work, we generated a hypomorphic allele of *dSarm* predicted to lack NAD^+ hydrolase activity, $dSarm^{E1170A}$. Whereas *dSarm* null mutants protect severed axons for weeks after axotomy (Osterloh et al., 2012; Neukomm et al., 2017), we found $dSarm^{E1170A}$ only protected severed axons for 5 days (Hsu et al., 2020). We therefore crossed strong *dWnk* alleles into this background and severed axons but found that $dSarm^{E1170A}$, $dWnk^{3L.282}$ MARCM clones displayed no increased protection after axotomy relative to $dSarm^{E1170A}$ alone at 10 dpa (Fig. 5C). These findings imply that, despite dNmnat loss occurring in both contexts, dWnk loss is not sufficient to protect severed distal axons or even enhance weaker *dSarm* phenotypes in the context of axotomy.

Given that introduction of activated $Fray^{S347D}$ can overcome *dSarm* null mutant neuroprotection against dNmnat depletion, we asked whether it would similarly bypass the protection afforded by $dSarm^{896}$ null mutations in distal severed axons after axotomy. Surprisingly, we found that $Fray^{S347D}$ expression did not override the protection of distal severed axons in $dSarm^{896}$ null mutants even 10 dpa (Fig. 5C). We envision two possible explanations for these observations: (1) dNmnat depletion and axotomy are not equivalent with respect to neurodegenerative signaling and dWnk/Fray are only required after dNmnat depletion; or (2) that the ability of dWnk/Fray signaling may require the presence of the neuronal cell body to promote neurodegeneration.

Discussion

Understanding signaling pathways that sense neuronal dysfunction and then promote neurodegeneration will be a prerequisite to developing effective therapeutic approaches to block neuronal loss in patients. In this study, we identified a new role of *dWnk* in promoting neurodegeneration caused by dNmnat depletion, which also serves as a primary activator of the dSarm/SARM1 pro-degenerative pathway. Our data support a model whereby dWnk signals through Fray to trigger neurodegeneration, but perhaps not ultimately through canonical Fray/SPAK/OSR1 downstream targets (e.g. KCCs/NKCCs). dWnk/Fray signal in parallel to dSarm and therefore represent a new branch of the neurodegeneration pathway activated upon dNmnat loss. Ultimately, dSarm and dWnk signaling converge on Axed, which remains absolutely required to promote degeneration of neurons after axotomy or dNmnat depletion. This work highlights the complexity of neurodegeneration signaling pathways *in vivo*, and the WNK/SPAK/OSR1 pathway

as a promising and possible therapeutic target in combination with SARM1 blockade to achieve maximum protection against neurodegeneration.

dNmnat loss activates dWnk/Fray and dSarm, potential sensors of neuronal health

Our unbiased forward genetic screen for suppressors of neurodegeneration after dNmnat depletion led to identification of two loss-of-function alleles of *dWnk*. Our subsequent detailed genetic analysis supports the notion that dWnk promotes neurodegeneration through the downstream kinase Fray. We also identified a new allele of *dSarm* in our screen, indicating our screen indeed identifies important pro-degenerative molecules. Given the additivity of *dSarm* and *dWnk* null alleles, and our observation that an activated version of Fray can bypass the neuroprotective effects of *dSarm* nulls after dNmnat loss, we propose that dNmnat depletion activates two distinct neurodegenerative pathways: one is dSarm-dependent, the other is dWnk/Fray-dependent. How might dWnk be activated? WNKs are unique kinases in that they can directly activated by sensing Cl^- levels or osmolarity (Goldsmith and Rodan, 2023). More recently, the kinase domain from dWnk and mammalian WNK3 and WNK4 have also been shown to be directly inhibited by high levels of K^+, in the 80-180 mM range (i.e. in the range of physiological intracellular K^+) (Pleinis et al., 2021). Given that loss of dNmnat/NMNAT2 leads to a decrease in NAD^+ and then ATP, a simple model would be that dWnk is normally inhibited by physiological levels of intracellular K^+ and is then activated after energetic failure in neurons lacking dNmnat leads to a failure of the Na^+/K^+ ATPase. dWnk/WNKs could therefore serve as ionic and/or osmotic sensors in dysfunctional axons. dSarm/SARM1 at the same time acts as a metabolic sensor, directly sensing NAD^+ and NMN via binding to the auto-inhibitory ARM domain (Bratkowski et al., 2020; Figley et al., 2021). Thus, dWnk/WNKs might complement the metabolic sensor dSarm/SARM1 to enable neurons to measure both cellular pools of NAD^+ (and indirectly ATP) along with cellular ionic status (K^+ and Cl^-). Indeed, ouabain treatment, which inhibits the Na^+/K^+ pump, has been shown to activate the WNK pathway (Pleinis et al., 2021). Given that mutation of the Cl^- binding site in dWnk did not affect its ability to drive neurodegeneration after dNmnat loss, we would propose that K^+ might be the key intracellular ion that would activate pro-degenerative dWnk signaling.

Activation of the dSarm signaling pathway (via deletion of the ARM domain) is sufficient to drive neurodegeneration, but activation of dWnk or Fray can only promote neurodegeneration after the loss of dNmnat but not in healthy wild type axons. Null alleles of *dWnk* or *fray* also fail to suppress Wallerian degeneration. While both axotomy and $dNmnat^{RNAi}$ share a key feature—dNmnat depletion—there are several notable differences in each assay. Neurons expressing *dNmnat RNAi* experience a gradual decline in dNmnat enzyme levels, rather than an acute loss that might occur after axotomy. Indeed, our data comparing neuroprotective effects at 25°C versus 29°C (where dNmnat depletion is more severe) revealed that the neuroprotective effects of *dWnk* and *dSarm* deletion depend on the severity of dNmnat loss. Interestingly, while *dWnk* loss did not augment the protective effect of a NADase-dead *dSarm* allele after injury, it did enhance neuroprotection in the context of dNmnat depletion (data not shown). Moreover, expressing activated dWnk or Fray reduced the neuroprotective effects of *dSarm* null mutants in $dNmnat^{RNAi}$-expressing neurons but not in severed axons. It is possible that the neuroprotection of *dWnk* and *fray* mutants after dNmnat loss might require the presence of the neuronal cell body. Certainly, the ability of Fray to overcome the neuroprotective effects of *dSarm* nulls did only occur in intact neuron. Interestingly, a putative Fray binding partner, HDAC1, has recently been implicated in

regulating the retrograde transport of neurodegenerative signals from axon terminals to neuronal cell bodies (Pathak et al., 2018).

WNKs and SPAK/OSR1 are conserved regulators of neuronal development, function and pathology

WNKs, in conjunction with SPAK and OSR1, serve as key regulators of intracellular chloride homeostasis by modulating the activities of NKCCs and KCCs (Shekarabi et al., 2017; Goldsmith and Rodan, 2023). In mature central nervous system (CNS) neurons, low intracellular Cl^- concentrations are essential for GABA-mediated synaptic inhibition (Kahle et al., 2015; Tang et al., 2021). Mutations in members of the WNK pathway have been linked to neurodevelopmental disorders characterized by disrupted GABAergic signaling, including epilepsy, autism spectrum disorder, schizophrenia, and intellectual disability (Tang et al., 2021). Hereditary sensory and autonomic neuropathy type II (HSANII), a rare neurodegenerative condition, is caused by mutations in the HSN2 exon of *WNK1*. These mutations result in a truncated WNK1 protein that retains the kinase domain but lacks the C-terminal RFxV/I motif, necessary for binding the downstream targets (Rahmani et al., 2018). The mechanism by which this truncated WNK1 leads to neuronal loss during development remains unclear. In mouse models, removal of the HSN2 exon does not replicate the peripheral neuropathy seen in HSANII patients, suggesting that the presence of the truncated WNK1 protein may drive the neuropathy (Kahle et al., 2016). Similarly, in *Drosophila* the $dWnk^{F1183}$ allele, which results in defects in axon outgrowth and maintenance (Berger et al., 2008; Izadifar et al., 2021), produces a protein with an intact kinase domain lacking the C-terminal Fray-binding motif, and mimics the mutations causing HSANII (Rahmani et al., 2018). This allele also disrupts visual system wiring (Berger et al., 2008). The yet-to-be-identified changes in dWnk and WNK1 signaling caused by truncations, versus clean deletions, could explain why we did not observe neurodevelopmental defects in the $dWnk^{F1183}$ background, and why it failed to suppress neurodegeneration in our hands. We also note that neurodevelopmental defects associated with dWnk signaling did not require Fray (Izadifar et al., 2021), suggesting that pro-degenerative signaling may require Fray/SPAK/OSR1, which neurodevelopmental roles are mediated by an alternate downstream kinase.

Ischemic stroke is an acute condition characterized by extensive cell death in the ischemic core, which can activate the neuronal WNK pathway in the ischemic penumbra due to for example osmotic stress (Bhuiyan et al., 2020). Interestingly, deletion of *WNK3* or *SPAK* has been shown to reduce tissue damage, including neuronal loss, by inhibiting NKCC1 activation in mouse models of stroke (Begum et al., 2015; Zhao et al., 2017). In a primary cortical neuron ischemia/reperfusion model, NKCC1-dependent sodium influx triggers the reverse mode of the Na^+/Ca^{2+} exchanger (NCX (Chen et al., 2008)), raising intracellular Ca^{2+} levels—a well-known driver of neurodegeneration. Surprisingly, the loss of either of the two *Drosophila* NKCCs (ncc69 and NKCC) or any of the three Irk channels – the other family of potassium channels regulated by the WNK pathway –individually did not replicate the phenotypes observed with *dWnk* or *fray* loss. This could be the result of functional redundancy among the NKCC and Irk family members in the fly or suggest that alternate downstream signaling molecules drive neurodegeneration.

Materials and Methods

KEY RESOURCES TABLE

REAGENT or RESOURCE	SOURCE	IDENTIFIER
Chemicals, Peptides, and Recombinant Proteins		
Halocarbon Oil 27	Sigma	Cat# H8773
One Shot™ TOP 10 Chemically Competent *E. coli*	ThermoFisher	Cat# C404010
NEBuilder® HiFi DNA Assembly Master Mix	NEB	Cat# E2621S
Experimental models: *Drosophila melanogaster*		
OK371-gal4	Bloomington Drosophila Stock Center (BDSC)	BDSC# 26160
10xUAS-ivs-mCD8-GFP	BDSC	BDSC# 32186
10XUAS-myrTdTomato	BDSC	BDSC# 32222
5XUAS-dNmnat RNAi	Vienna Drosophila Resource Center (VDRC)	VDRC# v32255
5XUAS-dicer2	BDSC	BDSC# 24650
5XUAS-LacZ	BDSC	BDSC# 3956
aseFLP^{2e}	Freeman Lab (Neukomm et al., 2014)	N/A
aseFLP^{2c}	Freeman Lab (Neukomm et al., 2014)	N/A
OR22a-gal4	BDSC	BDSC# 9952
tub-gal80 FRT2A	BDSC	BDSC# 5190
tub-gal80 FRT80B	BDSC	BDSC# 5191
FRT82B tub-gal80	BDSC	BDSC# 5135
FRT82B	BDSC	BDSC# 2035
FRT80B	BDSC	BDSC# 1988
FRT2A	BDSC	BDSC# 1997
5XUAS-dSarm$^{\Delta ARM}$-myc	Freeman Lab (Neukomm et al., 2017)	N/A
tubP-GAL80^{ts}	BDSC	BDSC# 7019
dWnk$^{3L.282}$	This study	N/A
dWnk$^{3L.1541}$	This study	N/A
dWnk^{MB06499}	BDSC	BDSC# 26050
dWnk^{G1286}	(Berger et al., 2008)	N/A
dWnk^{F1183}	(Berger et al., 2008)	N/A
Df(3L)Exel9066	BDSC	BDSC# 7950
Df(3L)ED4978	(Ryder et al., 2007)	BDSC# 8101
5xUAS-dWnk^{WT}	This study	N/A
5xUAS-dWnk^{S632A}	This study	N/A
5xUAS-dWnk^{L619F}	This study	N/A
5xUAS-dWnk^{D618A}	This study	N/A
fray^{07551}CG7694^{07551}	(Russell et al., 1998)	BDSC# 11721
fray^{ywg2+}	This study	N/A
fray$^{\Delta}$	This study	N/A
fray^{K67M}	This study	N/A
nanos-Cas9.R	BDSC	BDSC# 78781
nanos-Cas9.P	BDSC	BDSC# 54591
5xUAS-Fray^{D185A}	This study	N/A
5xUAS-Fray^{S347D}	This study	N/A
5xUAS-Fray^{T206E}	This study	N/A
dSarm^{E1170A}	Freeman Lab (Hsu et al., 2020)	N/A
dSarm^{896}	Freeman Lab (Osterloh et al., 2012)	N/A
axed$^{3L.11}$	Freeman Lab (Neukomm et al., 2017)	N/A
Oligonucleotides		
Recombinant DNA		
LD15845	Drosophila Genomics Resource Centre (DGRC)	RRID:DGRC_5048
pCFD3-dU6:3gRNA	Addgene	Cat# 49410

pBH vector	Bellen Lab	N/A
pBH-5'HMA-y^{wing}-3'HMA (*fray* locus)	This study	N/A
pBH-5'HMA-frayK67M-3'HMA	This study	N/A
pattB-5xUAS-$dWnk^{WT}$	This study	N/A
pattB-5xUAS-$dWnk^{S632A}$	This study	N/A
pattB-5xUAS-$dWnk^{D618A}$	This study	N/A
pattB-5xUAS-$dWnk^{L619F}$	This study	N/A
pattB-5xUAS-$Fray^{WT}$	This study	N/A
pattB-5xUAS-$Fray^{S347D}$	This study	N/A
pattB-5xUAS-$Fray^{T206E}$	This study	N/A
pattB-5xUAS-$Fray^{D185A}$	This study	N/A
Software and algorithms		
Fiji	ImageJ	N/A
Zen 3.9	Zeiss	N/A
Prism 10	GraphPad	N/A
Illustrator for Biological Sequences (IBS)	(Xie et al., 2022)	http://ibs.biocuckoo.org
Tools		

RESOURCE AVAILABILITY

Leading contact

Further information and requests for resources and reagents should be directed to and will be fulfilled by the Lead Contact Marc R. Freeman (freemmar@ohsu.edu).

Materials availability

All unique reagents generated in this study are available from the Lead Contact without restriction.

Data and code availability

This study did not generate any unique datasets or code.

EXPERIMENTAL MODEL AND SUBJECT DETAILS

Animals

Flies (*D. melanogaster*) were maintained on standard cornmeal agar supplemented with dry yeast at 25°C for the experiments presented in Figures 1-3 & 5C. For Figures 4 and 5A, flies were kept at 25°C for 3-4 days, after which the parents were transferred to fresh vials, and the progeny were raised at 29°C until imaging. *Nmnat KD*-induced neurodegeneration was more robust in females, so equal numbers of males and females were included in each experiment. The full list of fly lines used in this study is provided in the Key Resources Table, and the specific genotypes used for each figure are provided in Supplementary Table 3 and 4.

METOD DETAILS

Axotomy assays

Flies (5-6 days old) were anesthetized on a CO_2 pad, and the L1 wing vein was cut at the midpoint, just above the posterior cross-vein, using MicroPoint scissors. After the injury, the flies were returned to vials and incubated at 25°C. The wings were dissected for imaging 10 days post-axotomy.

For the *dSarm*^{896} + *UAS-Fray*^{S347D} experiment, flies were raised at 29°C for 8 days before the L1 wing vein was cut in the middle with MicroPoint scissors. After the injury, flies were returned to vials and incubated at 25°C. The wings were dissected for imaging 10 days post-axotomy.

dSarm$^{\Delta ARM}$ expression in adults

Virgin females of *5xUAS-dSarm*$^{\Delta ARM}$*-myc*, *tub-gal80*^{ts}*/CyO*; *tub-gal80 FRT2A* (or *FRT82B tub-gal80)/TM3, Sb*^{1} genotype were crossed to MARCM-ready males bearing *dWnk*$^{3L.282}$ or *fray*^{07551} alleles, respectively. The crosses were incubated at 18°C (where Gal80 is active, thus halting Gal4-mediated expression). Eclosed progeny of the correct genotype were shifted to 29°C (where Gal80 is inactive) to induce Gal4-mediated expression of dSarm$^{\Delta ARM}$. Complete neurodegeneration in control backgrounds was observed after 7 days at 29°C, which was selected as the experimental time point.

5xUAS-dWnk^{WT}, 5xUAS-dWnk^{S632A}, 5xUAS-dWnk^{D618A} and 5xUAS-dWnk^{L619F} cloning and transgenesis

The open reading frame of the longest dWnk transcript was synthesized by Genewiz and the puc57-wnk vector served as the starting template for all dWnk cloning. For targeted mutagenesis, base pairs 1259-2751 of the dWnk sequence, which contain all sites intended for mutation, were PCR-amplified while incorporating KpnI and XbaI sites at the 5' and 3' ends, respectively. The amplified fragment was then cloned into the pSK vector using KpnI/XbaI restriction sites. Specific mutations were introduced at desired sites within this region of dWnk using the QuikChange II-E Site-Directed Mutagenesis Kit. Primers used for this process are listed in the Key Resources Table. Mutagenized fragments were confirmed by sequencing, after which the targeted fragments were excised using NheI and BstBI restriction enzymes and cloned back into the puc57-wnk vector. To insert dWnk sequences into the pattB-5xUAS vector, the dWnk sequence was removed from puc57-wnk using NotI and KpnI restriction enzymes and then cloned into the pattB-5xUAS vector. The DNA was injected into *y*^{1} *w*^{67c23} *P{CaryP}attP18* (RRID:BDSC_32107) and *y1 w*^{67c23}*; P{CaryP}attP154* flies by BestGene.

5xUAS-Fray^{WT}, 5xUAS-Fray^{D185A}, 5xUAS-Fray^{S347D} and 5xUAS-Fray^{T206E} cloning and transgenesis

To create Fray constructs, the pBluescript (BS)-Fray (LD15845 cDNA clone, see Key Resources Table) was used as a template. To generate the Fray^{WT} construct, Fray sequence was PCR-amplified from pBS-Fray with adding a NotI restriction site and a Kozak sequence to the 5' end and a KpnI site to the 3' end. The amplified Fray fragment was then cloned into the NotI and KpnI sites of the pattB-5xUAS vector. Specific mutations were introduced into Fray sequence using the QuikChange II-E Site-Directed Mutagenesis Kit. Primers used for this process are listed in the Key Resources Table. Once the mutation was confirmed, Fray sequence was excised from pBS-Fray using NotI and KpnI and cloned it into the pattB-5xUAS vector. The DNA was injected into *y*^{1} *w*^{67c23} *P{CaryP}attP18* (RRID:BDSC_32107) and *y1 w*^{67c23}*; P{CaryP}attP154* flies by BestGene.

Generation of *fray*^{K67M} and *fray*$^{\Delta}$ flies

The *fray*^{K67M} and *fray*$^{\Delta}$ fly lines were generated following a previously described protocol (Li-Kroeger et al., 2018). A 1560 bp region containing the DNA sequence of *fray* exon 2 and 7 bp of the 3'UTR was selected for replacement with the *ywing2+* cassette. To construct the donor DNA (pBH-5'HMA-p{ywing2+}-3'HMA), the homology arms (HMA) were PCR-amplified from the genomic DNA of *y*^{1} *sc* v*^{1} *sev*^{21}*; P{nanos-Cas9.R}attP40/CyO* flies. Primers used for this process are listed in the Key Resources Table. The homology arms, pBH donor vector, and *p{y*$^{wing2+}$*}* were

combined using NEBuilder® HiFi DNA Assembly Master Mix with the BbsI restriction enzyme. The final product was confirmed by sequencing.

For the generation of sgRNA, standard cloning protocols were followed using the pCFD3-dU6:3gRNA plasmid (https://www.crisprflydesign.org). Briefly, sense and antisense oligos containing the 20 bp guide target sequence were annealed and cloned into the BbsI-cut pCFD3-dU6:3gRNA plasmid.

To generate the *fray*$^{ywg2+}$ flies, a mixture of 25 ng/ml sgRNA and 150 ng/ml donor DNA was injected into *y*^{1} *sc* v*^{1} *sev*^{21}*; P{nanos-Cas9.R}attP40/CyO* flies by Bestgene. The injected animals were then crossed to *yw* flies. Offspring were screened for yellow+ wings and crossed to the appropriate balancer flies. The entire homology arm sequence and about 200 bp of adjacent cassette sequences were verified by sequencing. Verified stocks were recombined to the *FRT82B* chromosome and tested for protection against *dNmnat KD*.

To replace the *y*$^{wing2+}$ cassette with the frayK67M sequence, donor DNA containing the K67M mutation (pBH-5'HMA-frayK67M-3'HMA) was generated (primers listed in the Key Resources Table). Briefly, primers containing the mutated nucleotides were used to amplify DNA fragments (5pHMA-frayK67M for the first half and frayK67M-3pHMA for the second half). NEBuilder® HiFi DNA Assembly Master Mix was used to combine all DNA fragments with the BbsI-cut pBH vector. sgRNA was generated as described above, using different 20 bp guide target sequences (Key Resources Table). A mixture of 25 ng/ml sgRNA and 150 ng/ml donor DNA was injected into *y*^{1} *M{w*$^{+mC}$*=nos-Cas9.P}ZH-2A w*;; FRT82B fray*$^{ywg2+}$*/TM3,Sb* flies by BestGene. Progeny were screened for the loss of the yellow+ wing phenotype. These flies were balanced, and the entire replaced region was sequenced to confirm the absence of additional mutations. One of the screened stocks exhibited the complete removal of the *y*$^{wing2+}$ cassette without replacement by the frayK67M donor DNA, thus generating a null allele (*fray*$^{\Delta}$).

Figures and Figure legends

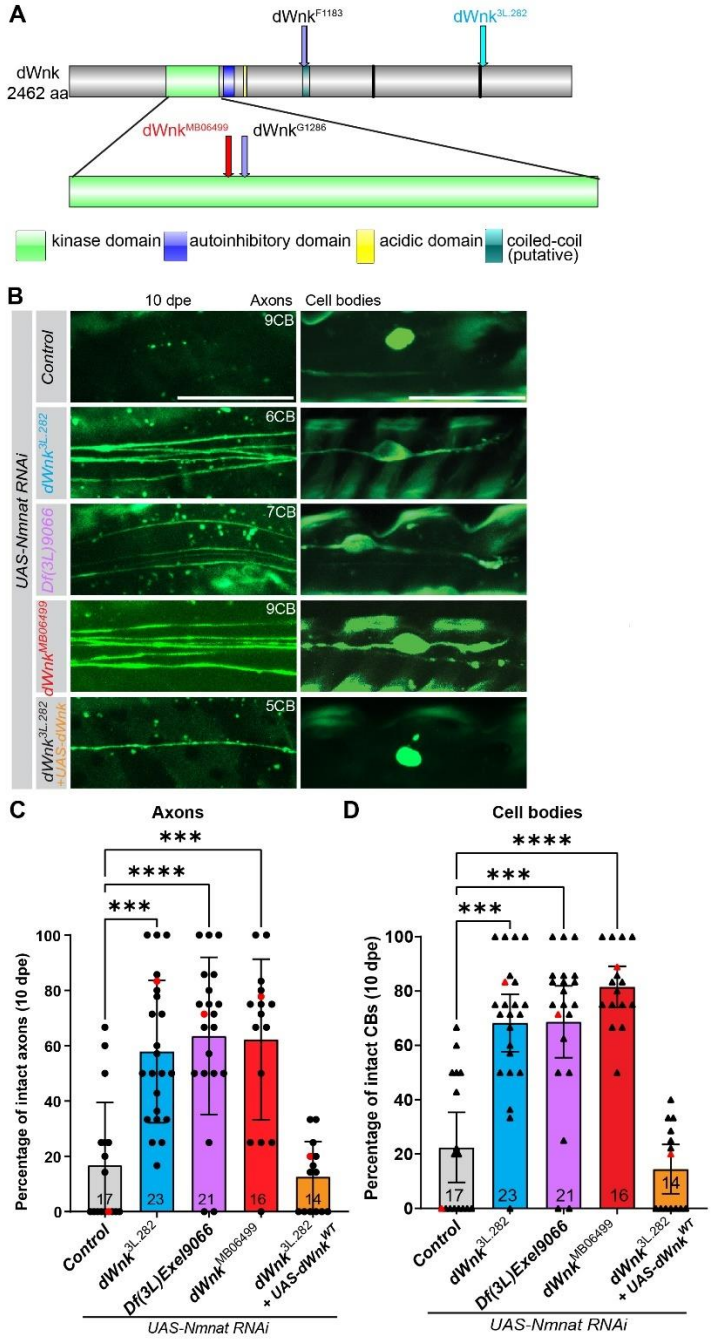

Figure 1. dWnk is a pro-degenerative gene.

(A) Schematic representation of the longest dWnk isoform (dWnk-PM, 2462 aa) showing the characterized and putative domains. The mutations used in this study are indicated. **(B)** Representative images of 10 dpe wings showing axonal protection of *dWnk* LOF and null alleles from *dNmnat KD*-induced neurodegeneration. Re-supply of dWnk into *dWnk*$^{3L.282}$ neurons restores their ability to degenerate following dNmnat depletion. Scale bar is 20 µm. **(C-D)** Quantifications of intact axons **(C)** and cell bodies **(D)** shown in B. Red dots and triangles represent the images in B. The results are plotted as mean ± 95% confidence interval (CI) and analyzed using Kruskal-Wallis tests with post-hoc Dunn's multiple comparison test. All comparisons are listed in the Supplementary table 1.

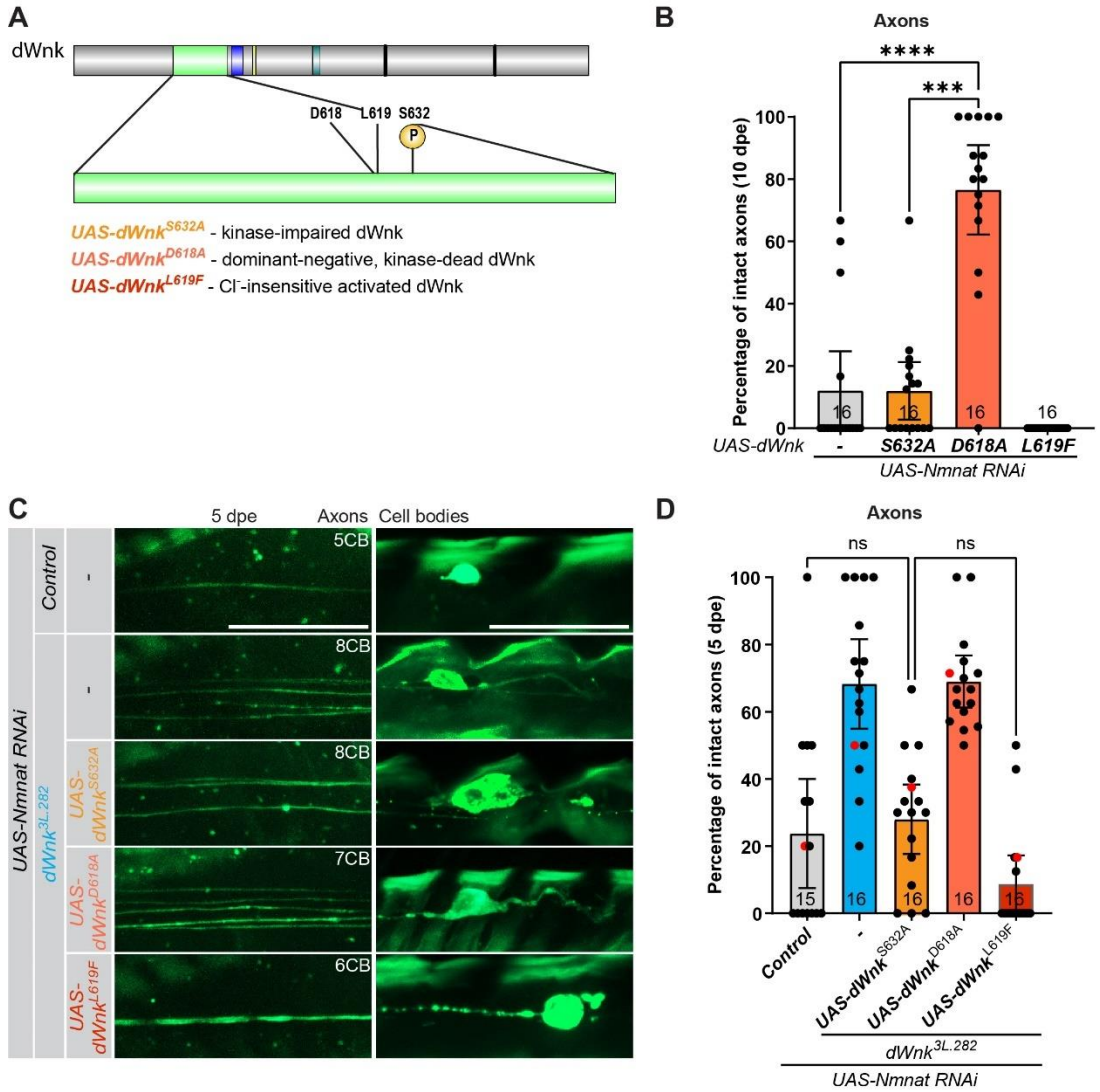
A
dWnk
D618
L619
S632
P
UAS-dWnkS632A - kinase-impaired dWnk
UAS-dWnkD618A - dominant-negative, kinase-dead dWnk
UAS-dWnkL619F - Cl⁻-insensitive activated dWnk
B
Axons
****
***
Percentage of intact axons (10 dpe)
100
80
60
40
20
0
16
16
16
16
UAS-dWnk
-
S632A
D618A
L619F
UAS-Nmnat RNAi
C
5 dpe
Axons
Cell bodies
UAS-Nmnat RNAi
dWnk3L.282
Control
-
-
UAS-dWnkS632A
UAS-dWnkD618A
UAS-dWnkL619F
5CB
8CB
8CB
7CB
6CB
D
Axons
ns
ns
Percentage of intact axons (5 dpe)
100
80
60
40
20
0
15
16
16
16
16
Control
-
UAS-dWnkS632A
UAS-dWnkD618A
UAS-dWnkL619F
dWnk3L.282
UAS-Nmnat RNAi

Figure 2. dWnk kinase activity is essential for driving *dNmnat KD*-induced neurodegeneration.

(A) Schematic representation of the kinase domain of dWnk, with the residues important for dWnk kinase activity indicated: D618 – ATP binding, L619 – chloride sensing, and S632 – first auto-phosphorylation site. **(B)** $dWnk^{D618A}$ is a dominant-negative form of dWnk. Quantifications show the neuroprotection provided by the expression of $dWnk^{D618A}$ against *dNmnat KD*-induced neurodegeneration (10 dpe). The results are plotted as mean ± 95% CI and analyzed using Kruskal-Wallis tests with post-hoc Dunn's multiple comparison test. All comparisons are listed in the Supplementary table 1. **(C)** Representative images of 5 dpe wings showing that the axonal protection provided by $dWnk^{3L.282}$ against *dNmnat KD*-induced neurodegeneration can be abolished by the re-supply of auto-activation impaired $dWnk^{S632A}$ or Cl^--insensitive $dWnk^{L619F}$, but not by dominant-negative, kinase-dead $dWnk^{D618A}$. Scale bar is 20 μm. **(D)** Quantifications of the experiments shown in C. The red dots represent the images in C. The results are plotted as mean ± 95% CI and analyzed using Kruskal-Wallis tests with post-hoc Dunn's multiple comparison test. All comparisons are listed in the Supplementary table 1.

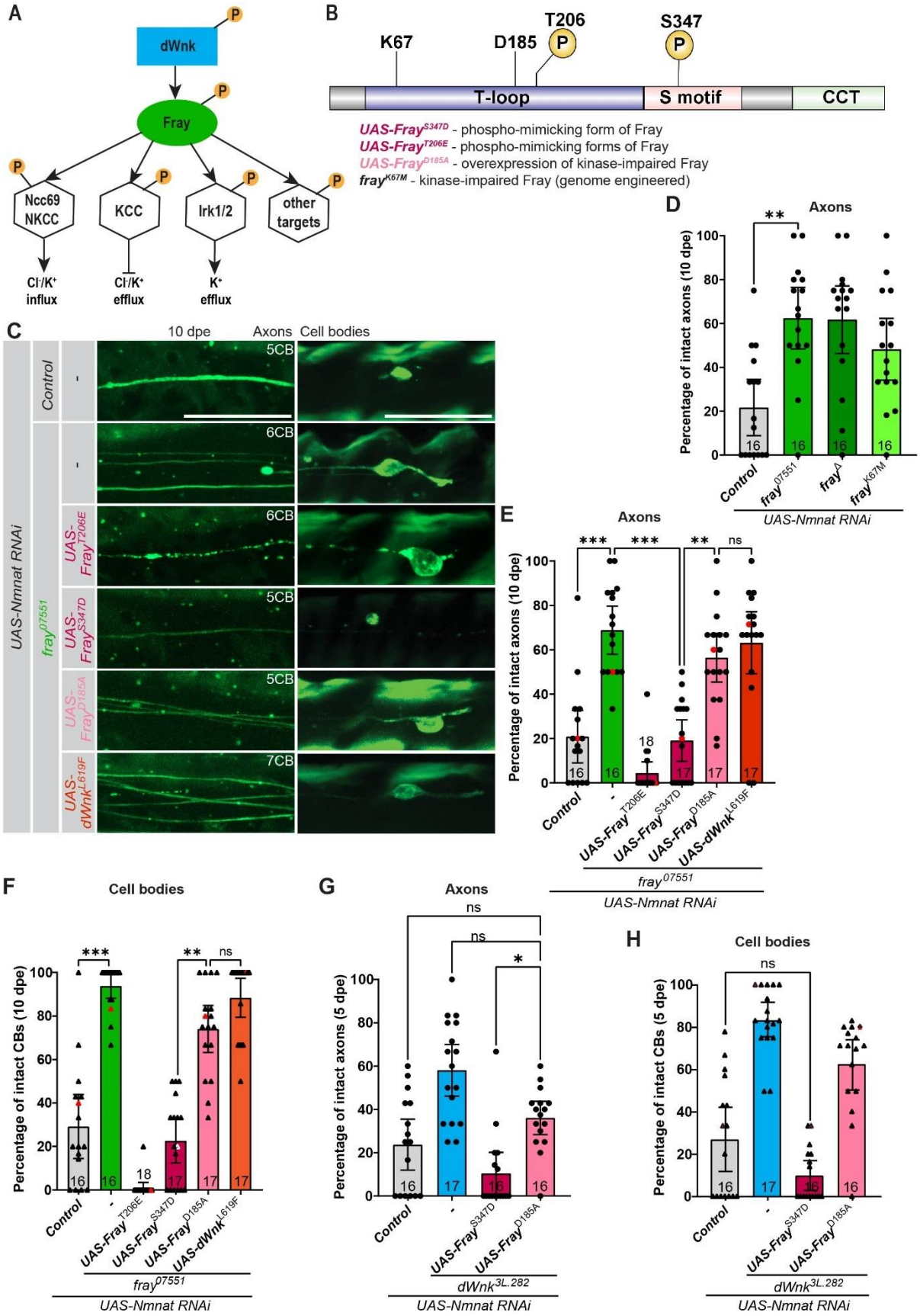
A
dWnk
P
Fray
Ncc69
NKCC
KCC
Irk1/2
other targets
Cl⁻/K⁺ influx
Cl⁻/K⁺ efflux
K⁺ efflux
B
K67
D185
T206
S347
T-loop
S motif
CCT
UAS-Fray S347D - phospho-mimicking form of Fray
UAS-Fray T206E - phospho-mimicking forms of Fray
UAS-Fray D185A - overexpression of kinase-impaired Fray
fray K67M - kinase-impaired Fray (genome engineered)
C
10 dpe
Axons
Cell bodies
UAS-Nmnat RNAi
Control
fray 07551
UAS-Fray T206E
UAS-Fray S347D
UAS-Fray D185A
UAS-dWnk L619F
5CB
6CB
7CB
D
Axons
Percentage of intact axons (10 dpe)
Control
fray 07551
fray Δ
fray K67M
UAS-Nmnat RNAi
E
Axons
Percentage of intact axons (10 dpe)
UAS-Fray T206E
UAS-Fray S347D
UAS-Fray D185A
UAS-dWnk L619F
fray 07551
UAS-Nmnat RNAi
F
Cell bodies
Percentage of intact CBs (10 dpe)
G
Axons
Percentage of intact axons (5 dpe)
dWnk 3L.282
H
Cell bodies
Percentage of intact CBs (5 dpe)

Figure 3. Fray kinase promotes *dNmnat KD*-induced neurodegeneration downstream of dWnk.

(A) The dWnk pathway: dWnk is activated by auto-phosphorylation. Fray is then phosphorylated by dWnk at the T-loop residue T206 and the S-motif residue S347. Activated Fray subsequently phosphorylates downstream targets. **(B)** Schematic representation of Fray, indicating the residues important for Fray kinase activity: K67 – catalytic lysine, D185 – ATP binding, and T206 & S347 – dWnk phosphorylation sites. **(C)** Representative images of 10 dpe wings showing the axonal protection provided by the *fray LOF* allele against *dNmnat KD*-induced neurodegeneration. Re-supplying phospho-mimicking forms of Fray, $Fray^{T206E}$ and $Fray^{S347D}$, but not the kinase-impaired form $Fray^{D185A}$, to $fray^{07551}$ neurons restores their ability to degenerate following dNmnat depletion. Expression of Cl^--insensitive dWnk, $dWnk^{L619F}$, in $fray^{07551}$ neurons does not abolish their protection from dNmnat depletion. Scale bar is 20 µm. **(D)** A LOF allele of *fray* in which the catalytic lysine (K67) of Fray was mutated to methionine protect neurons from dNmnat KD-induced neurodegeneration. The results are plotted as mean ± 95% CI and analyzed using Kruskal-Wallis tests with post-hoc Dunn's multiple comparison test. All comparisons are listed in the Supplementary table 1. **(E-F)** Quantifications of intact axons **(E)** and cell bodies **(F)** shown in panel C. The red dots and triangles represent the images C. The results are plotted as mean ± 95% CI and analyzed using Kruskal-Wallis tests with post-hoc Dunn's multiple comparison test. All comparisons are listed in the Supplementary table 1. **(G-H)** Expression of the phospho-mimicking form of Fray, $Fray^{S347D}$, abolishes the axonal **(G)** and cell body **(H)** protection provided by $dWnk^{3L.282}$ against dNmnat depletion (5 dpe). Expression of the kinase-impaired form of Fray, $Fray^{D185A}$, in $dWnk^{3L.282}$ neurons delays *dNmnat KD*-induced axonal **(G)** and cell body **(H)** loss (5 dpe). The results are plotted as mean ± 95% CI and analyzed using Kruskal-Wallis tests with post-hoc Dunn's multiple comparison test. All comparisons are listed in the Supplementary table 1.

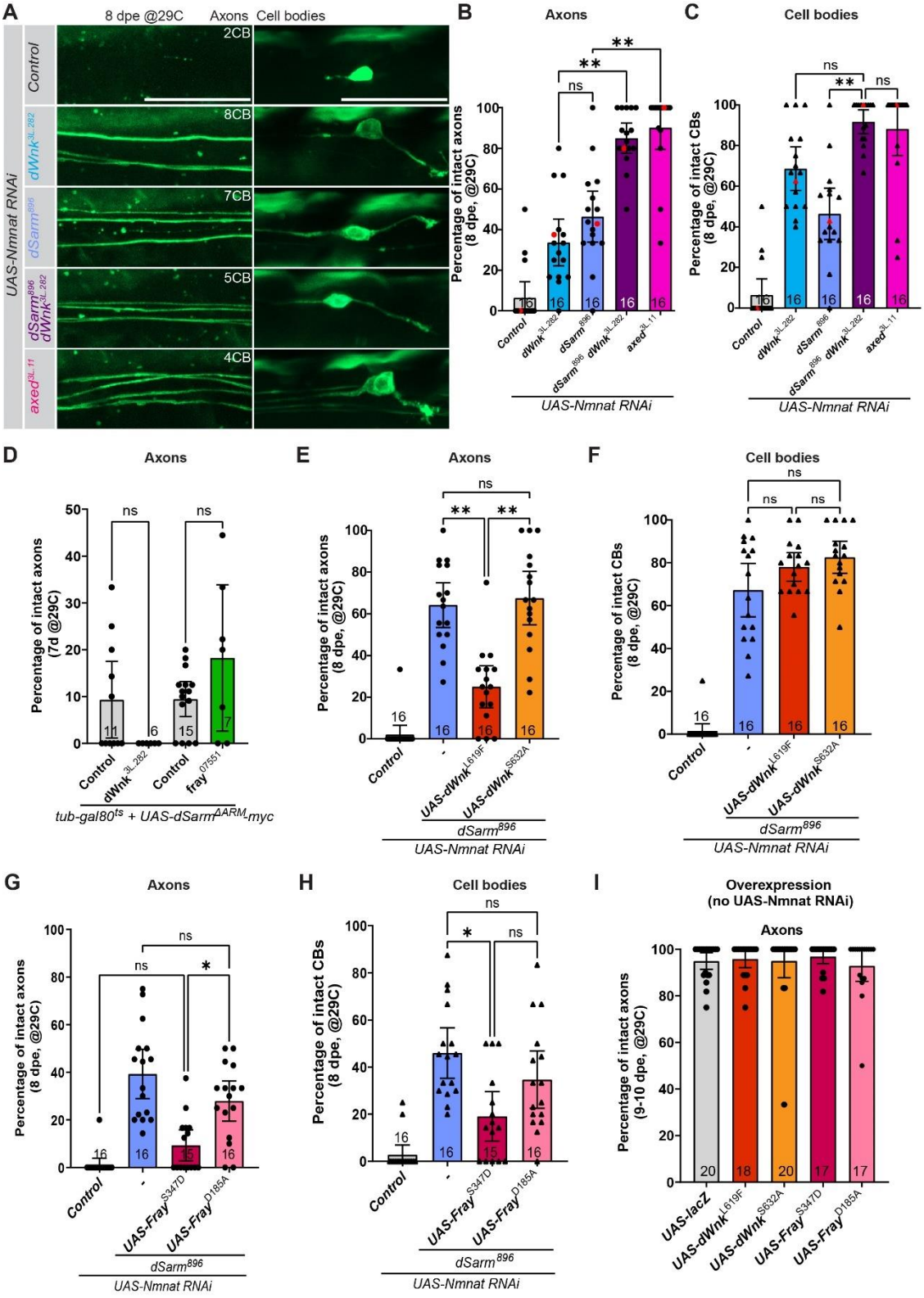
A
8 dpe @29C
Axons
Cell bodies
2CB
8CB
7CB
5CB
4CB
Control
dWnk3L.282
dSarm896
dSarm896 dWnk3L.282
axed3L.11
UAS-Nmnat RNAi
B
Axons
Percentage of intact axons (8 dpe, @29C)
ns
**
**
Control
dWnk3L.282
dSarm896
dSarm896 dWnk3L.282
axed3L.11
UAS-Nmnat RNAi
C
Cell bodies
Percentage of intact CBs (8 dpe, @29C)
ns
**
ns
Control
dWnk3L.282
dSarm896
dSarm896 dWnk3L.282
axed3L.11
UAS-Nmnat RNAi
D
Axons
Percentage of intact axons (7d @29C)
ns
ns
Control
dWnk3L.282
Control
fray07551
tub-gal80ts + UAS-dSarmΔARM-myc
E
Axons
Percentage of intact axons (8 dpe, @29C)
ns
**
**
Control
-
UAS-dWnkL619F
UAS-dWnkS632A
dSarm896
UAS-Nmnat RNAi
F
Cell bodies
Percentage of intact CBs (8 dpe, @29C)
ns
ns
ns
Control
-
UAS-dWnkL619F
UAS-dWnkS632A
dSarm896
UAS-Nmnat RNAi
G
Axons
Percentage of intact axons (8 dpe, @29C)
ns
ns
*
Control
-
UAS-FrayS347D
UAS-FrayD185A
dSarm896
UAS-Nmnat RNAi
H
Cell bodies
Percentage of intact CBs (8 dpe, @29C)
ns
*
ns
Control
-
UAS-FrayS347D
UAS-FrayD185A
dSarm896
UAS-Nmnat RNAi
I
Overexpression (no UAS-Nmnat RNAi)
Axons
Percentage of intact axons (9-10 dpe, @29C)
UAS-lacZ
UAS-dWnkL619F
UAS-dWnkS632A
UAS-FrayS347D
UAS-FrayD185A

Figure 4. dWnk acts in parallel to dSarm upon dNmnat depletion.

(A) Representative images of 8 dpe wings show partial axonal protection by the *dWnk*$^{3L.282}$ and *dSarm*^{896} alleles against robust *dNmnat KD*-induced neurodegeneration (29°C). *dSarm*^{896}*,dWnk*$^{3L.282}$ double mutant neurons are protected to the same extent as *axed* KO neurons. *dWnk*$^{3L.282}$ protects neuronal cell bodies from strong dNmnat depletion better than *dSarm*^{896}. Neuronal cell bodies in the *dSarm*^{896}*,dWnk*$^{3L.282}$ double mutant are completely protected, similar to *axed* KO. **(B-C)** Quantifications of the experiments in A: axonal protection is shown in panel B, and cell body protection in panel C. Red dots **(B)** and triangles **(C)** represent the images in panel A. The results are plotted as mean ± 95% CI and analyzed using Kruskal-Wallis tests with post-hoc Dunn's multiple comparison test. All comparisons are listed in the Supplementary table 1. **(D)** Loss of either *dWnk* or *fray* does not protect against neurodegeneration caused by dSarm$^{\Delta ARM}$ expression. The results are plotted as mean ± 95% CI and analyzed using Kruskal-Wallis tests with post-hoc Dunn's multiple comparison test. All comparisons are listed in the Supplementary table 1. **(E-F)** Over-activation of the dWnk/Fray branch by expressing Cl^--insensitive dWnk (dWnk^{L619F}), but not auto-activation impaired dWnk (dWnk^{S632A}), in neurons decreases the axonal protection **(E)** provided by *dSarm*^{896} against dNmnat depletion. Overexpression of either form of dWnk did not reduce the cell body protection **(F)** provided to *dSarm*^{896} neurons against dNmnat depletion. The results are plotted as mean ± 95% CI and analyzed using Kruskal-Wallis tests with post-hoc Dunn's multiple comparison test. All comparisons are listed in the Supplementary table 1. **(G-H)** Over-activation of the dWnk/Fray branch by expressing the phospho-mimicking form of Fray (Fray^{S347D}), but not the kinase-impaired form (Fray^{D185A}), in *dSarm*^{896} neurons decreases axonal **(G)** and cell body **(H)** protection from dNmnat depletion. The results are plotted as mean ± 95% CI and analyzed using Kruskal-Wallis tests with post-hoc Dunn's multiple comparison test. All comparisons are listed in the Supplementary table 1. **(I)** Strong overexpression of dWnk^{L619F}, dWnk^{S632A}, Fray^{S347D} and Fray^{D185A} without *dNmnat KD* does not cause neurodegeneration. The results are plotted as mean ± 95% CI. Data analysis is provided in the Supplementary table 1.

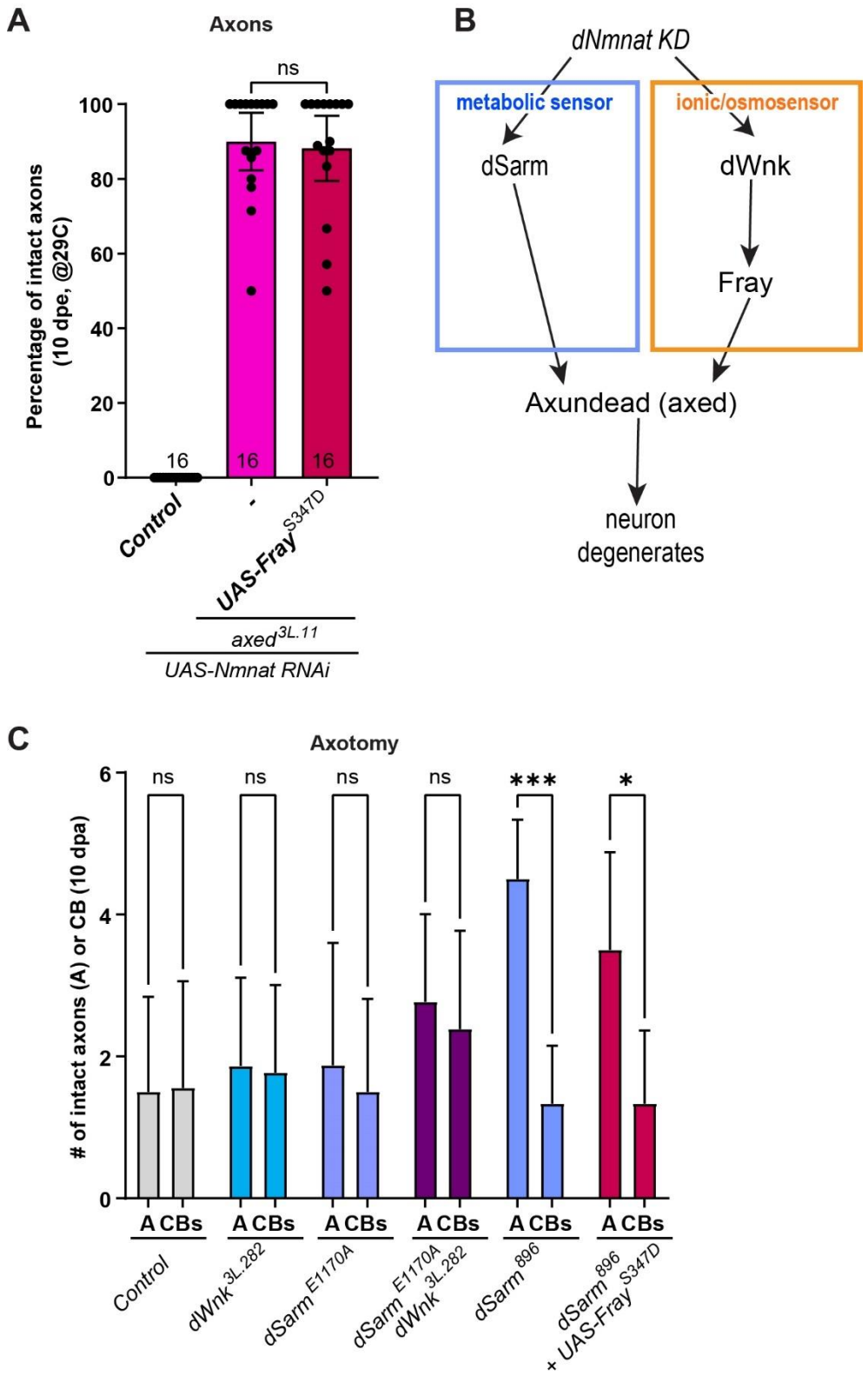
A
Axons
ns
Percentage of intact axons (10 dpe, @29C)
100
80
60
40
20
0
16
16
16
Control
-
UAS-Fray S347D
axed 3L.11
UAS-Nmnat RNAi
B
dNmnat KD
metabolic sensor
ionic/osmosensor
dSarm
dWnk
Fray
Axundead (axed)
neuron degenerates
C
Axotomy
# of intact axons (A) or CB (10 dpa)
6
4
2
0
ns
ns
ns
ns
***
*
A CBs
A CBs
A CBs
A CBs
A CBs
A CBs
Control
dWnk 3L.282
dSarm E1170A
dSarm E1170A dWnk 3L.282
dSarm 896
dSarm 896 + UAS-Fray S347D

Figure 5. The action of dWnk/Fray branch might require the presence of neuronal cell body.

(A) Strong expression of the phospho-mimicking form of Fray, Fray^{S347D}, does not eliminate the neuroprotection provided by *axed*$^{3L.11}$. The results are plotted as mean ± 95% CI and analyzed using Kruskal-Wallis tests with post-hoc Dunn's multiple comparison test. All comparisons are listed in the Supplementary table 1. **(B)** Both branches of neurodegeneration activated by dNmnat depletion converge on Axed, which executes neurodegeneration. **(C)** Loss of *dWnk* does not protect severed axons from degeneration and does not enhance the protection provided by the *dSarm* hypomorph allele (*dSarm*^{E1170A}). Strong expression of the phospho-mimicking form of Fray, Fray^{S347D}, does not diminish the protection of severed axons provided by the null allele of *dSarm* (*dSarm*^{896}). The results are plotted as mean ± SD and analyzed using 2way ANOVA with Šídák's multiple comparisons test. *** - p-value 0.0001 to 0.001, * - p-value 0.01 to 0.05, ns - p-value ≥ 0.05.

Supplementary Figures

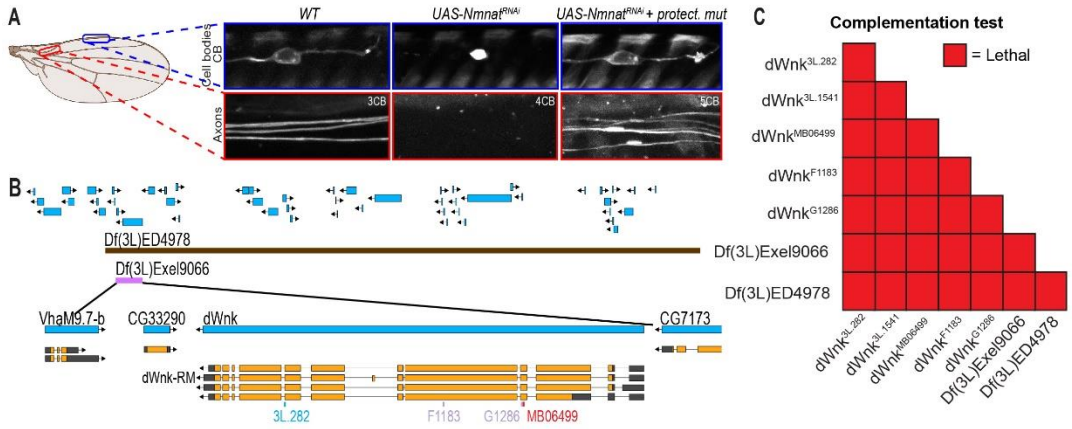

D

Nature of the dWnk alleles used for validation:

dWnk$^{3L.282}$	EMS, splice donor site	LOF
dWnk^{MB06499}	Minos transposon insertion	Null
dWnk^{G1286}	EMS, S556F	LOF
dWnk^{F1183}	EMS, Q1151Term	LOF
dWnk$^{3L.1541}$	EMS, regulatory region?	LOF
Df(3L)Exel9066	genomic deletion	Null

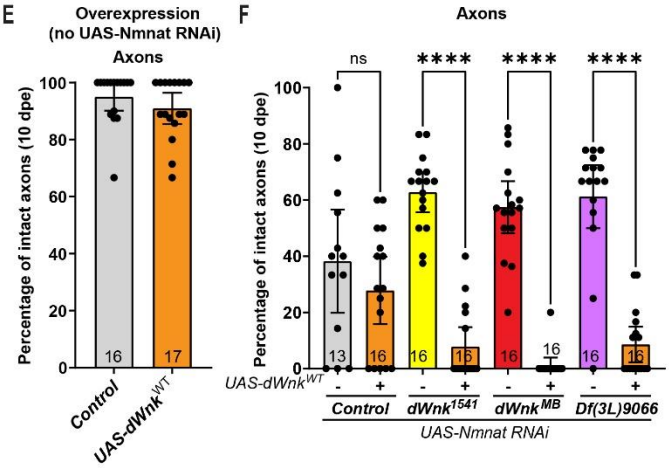

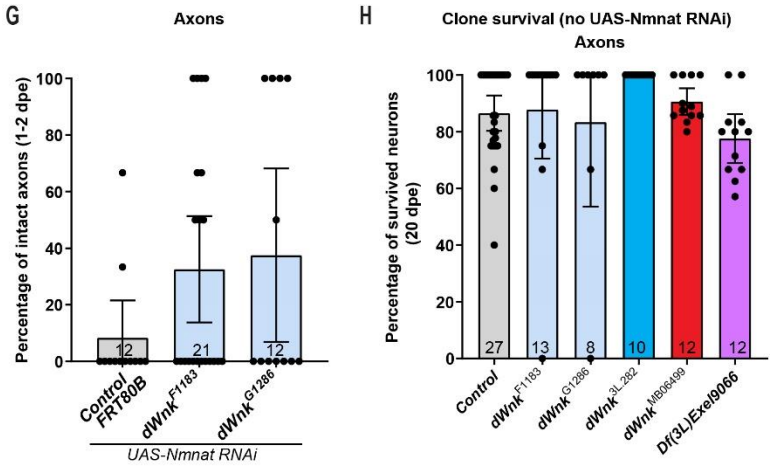

Figure S1.

(A) Schematics of the *dNmnat KD* screen: red insets represent images of distal axons, and blue insets – images of neuronal cell bodies. dNmnat depletion drives neurodegeneration. Protective backgrounds offer protection to both axons and cell bodies. **(B)** Schematic representation of the *dWnk* genomic locus, showing the genomic deletions and *dWnk* alleles used in this study. **(C)** Complementation tests with LOF and null alleles of *dWnk* indicate that $dWnk^{3L.282}$ and $dWnk^{3L.1541}$ are LOF alleles. **(D)** The nature of the *dWnk* LOF and *null* alleles used in this study. **(E)** Overexpression of $dWnk^{WT}$ without *dNmnat KD* does not cause neurodegeneration. The results are plotted as mean ± 95% CI. Data analysis is provided in the Supplementary table 2. **(F)** Re-supply of $dWnk^{WT}$ into $dWnk^{3L.1541}$, $dWnk^{MB06499}$, and *Df(3L)Exel9066* neurons restores their ability to degenerate following dNmnat depletion. The results are plotted as mean ± 95% CI and analyzed using Kruskal-Wallis tests with post-hoc Dunn's multiple comparison test. All comparisons are listed in the Supplementary table 2. **(G)** $dWnk^{G1286}$ and $dWnk^{F1183}$ alleles did not provide neuroprotection against dNmnat depletion. The results are plotted as mean ± 95% CI. Data analysis is provided in the Supplementary table 2. **(H)** Neurons homozygous for $dWnk^{G1286}$, $dWnk^{F1183}$, $dWnk^{3L.282}$, $dWnk^{MB06499}$ and *Df(3L)Exel9066* do not degenerate at 20 dpe. The results are plotted as mean ± 95% CI. Data analysis is provided in the Supplementary table 2.

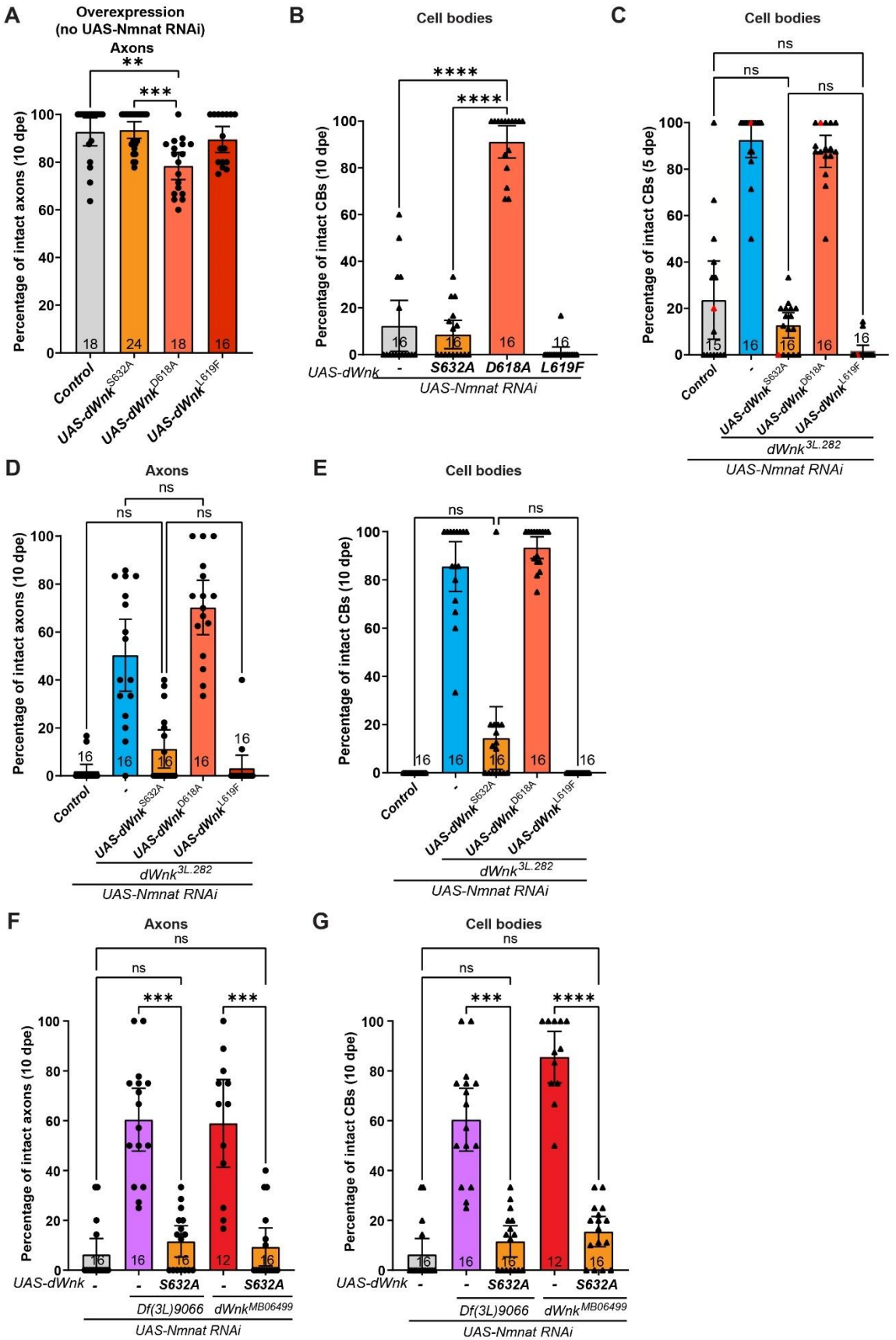
A
Overexpression
(no UAS-Nmnat RNAi)
Axons
Percentage of intact axons (10 dpe)
Control
UAS-dWnk S632A
UAS-dWnk D618A
UAS-dWnk L619F
B
Cell bodies
Percentage of intact CBs (10 dpe)
UAS-dWnk
S632A
D618A
L619F
UAS-Nmnat RNAi
C
Cell bodies
Percentage of intact CBs (5 dpe)
dWnk 3L.282
UAS-Nmnat RNAi
D
Axons
Percentage of intact axons (10 dpe)
E
Cell bodies
Percentage of intact CBs (10 dpe)
F
Axons
Percentage of intact axons (10 dpe)
Df(3L)9066
dWnk MB06499
G
Cell bodies
Percentage of intact CBs (10 dpe)

Figure S2.

(A) Overexpression of dWnk^{S632A} and dWnk^{L619F} without *dNmnat KD* does not cause neurodegeneration. Overexpression of dWnk^{D618A} without *dNmnat KD* slightly reduces neuronal viability. The results are plotted as mean ± 95% CI and analyzed using Kruskal-Wallis tests with post-hoc Dunn's multiple comparison test. All comparisons are listed in the Supplementary table 2. **(B)** Quantifications showing the neuronal cell body protection provided by the expression of dWnk^{D618A} against *dNmnat KD* (10 dpe, related to Fig. 2B). The results are plotted as mean ± 95% CI and analyzed using Kruskal-Wallis tests with post-hoc Dunn's multiple comparison test. All comparisons are listed in the Supplementary table 2. **(C)** Re-supplying the kinase-dead dWnk^{D618A} cannot erase the cell body protection provided by the *dWnk$^{3L.282}$* allele (5 dpe). Red triangles represent the images in Fig. 2C. The results are plotted as mean ± 95% CI and analyzed using Kruskal-Wallis tests with post-hoc Dunn's multiple comparison test. All comparisons are listed in the Supplementary table 2. **(D-E)** Expression of the kinase-dead dWnk^{D618A} does not erase the axonal **(D)** and cell body **(E)** protection provided by the *dWnk$^{3L.282}$* allele, even at 10 dpe. In contrast, expression of either dWnk^{S632A} or dWnk^{L619F} completely erases the axonal **(D)** and cell body **(E)** protection provided by *dWnk$^{3L.282}$* by 10 dpe. The results are plotted as mean ± 95% CI and analyzed using Kruskal-Wallis tests with post-hoc Dunn's multiple comparison test. All comparisons are listed in the Supplementary table 2. **(F-G)** Expression of auto-activation impaired dWnk^{S632A} completely erased the axon **(F)** and cell body **(G)** protection provided by either *dWnk^{MB06499}* or *Df(3L)Exel9066* by 10 dpe. The results are plotted as mean ± 95% CI and analyzed using Kruskal-Wallis tests with post-hoc Dunn's multiple comparison test. All comparisons are listed in the Supplementary table 2.

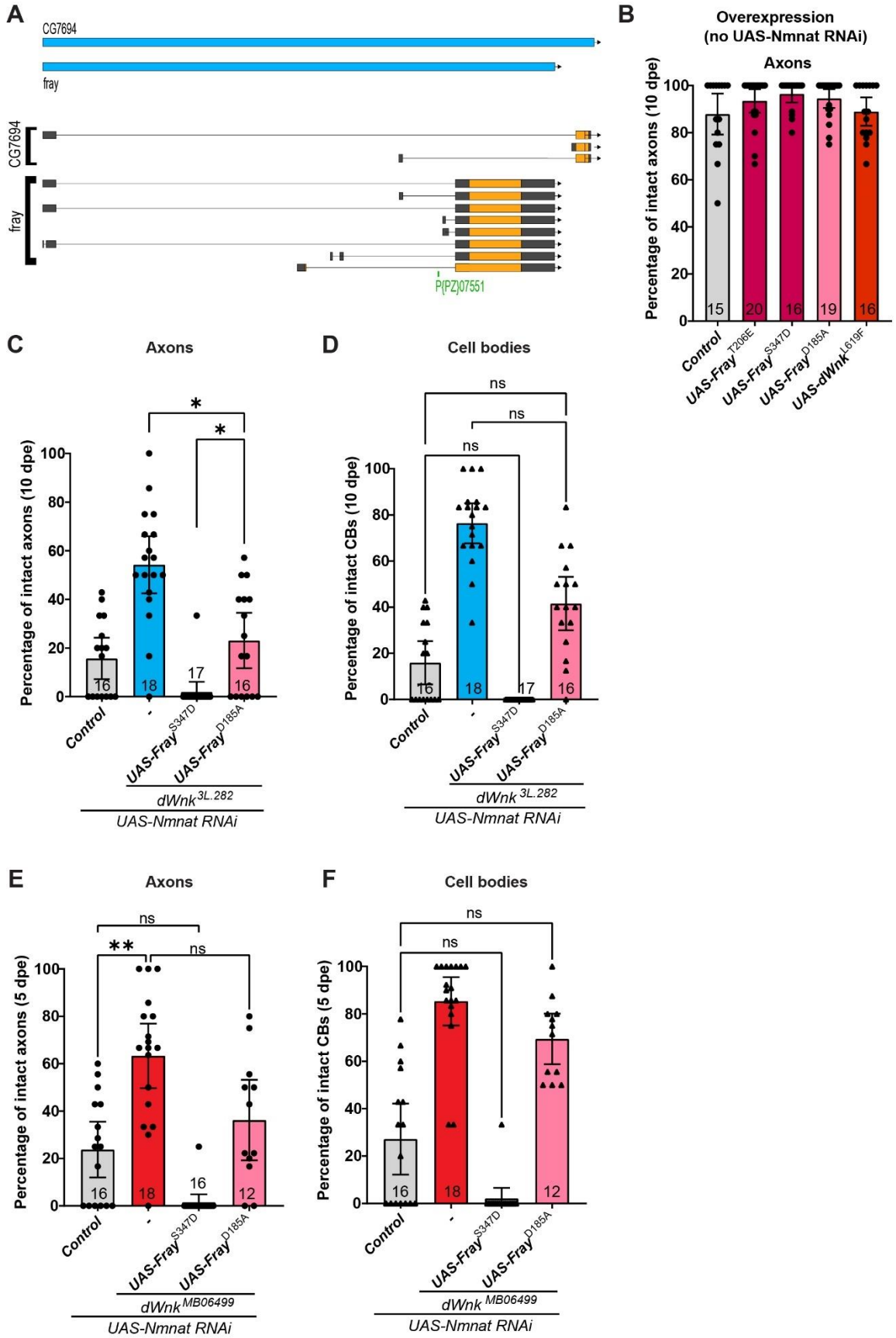
A
CG7694
fray
CG7694
fray
P{PZ}07551
B
Overexpression
(no UAS-Nmnat RNAi)
Axons
Percentage of intact axons (10 dpe)
Control
UAS-Fray T206E
UAS-Fray S347D
UAS-Fray D185A
UAS-dWnk L619F
C
Axons
Percentage of intact axons (10 dpe)
D
Cell bodies
Percentage of intact CBs (10 dpe)
ns
dWnk 3L.282
UAS-Nmnat RNAi
E
Axons
Percentage of intact axons (5 dpe)
F
Cell bodies
Percentage of intact CBs (5 dpe)
dWnk MB06499
UAS-Nmnat RNAi

Figure S3:

(A) Schematic representation of the *fray* locus, indicating the *fray*^{07551} allele used in this study. **(B)** Overexpression of Fray^{T206E}, Fray^{S347D}, Fray^{D185A} and dWnk^{L619F} without *dNmnat KD* does not cause neurodegeneration by 10 dpe. The results are plotted as mean ± 95% CI. Data analysis is provided in the Supplementary table 2. **(C-D)** Expression of Fray^{S347D} completely erases the axonal **(C)** and cell body **(D)** protection provided by *dWnk*$^{3L.282}$ by 10 dpe. Expression of Fray^{D185A} in *dWnk*$^{3L.282}$ neurons significantly delays axonal **(D)** and cell body **(E)** degeneration at 10 dpe. The results are plotted as mean ± 95% CI and analyzed using Kruskal-Wallis tests with post-hoc Dunn's multiple comparison test. All comparisons are listed in the Supplementary table 2. **(E-F)** Expression of Fray^{S347D} completely erases the axonal **(E)** and cell body **(F)** protection provided by *dWnk*^{MB06499} by 5 dpe. Expression Fray^{D185A}, in *dWnk*^{MB06499} neurons significantly delays axonal **(E)** and cell body **(F)** degeneration at 5 dpe. The results are plotted as mean ± 95% CI and analyzed using Kruskal-Wallis tests with post-hoc Dunn's multiple comparison test. All comparisons are listed in the Supplementary table 2.

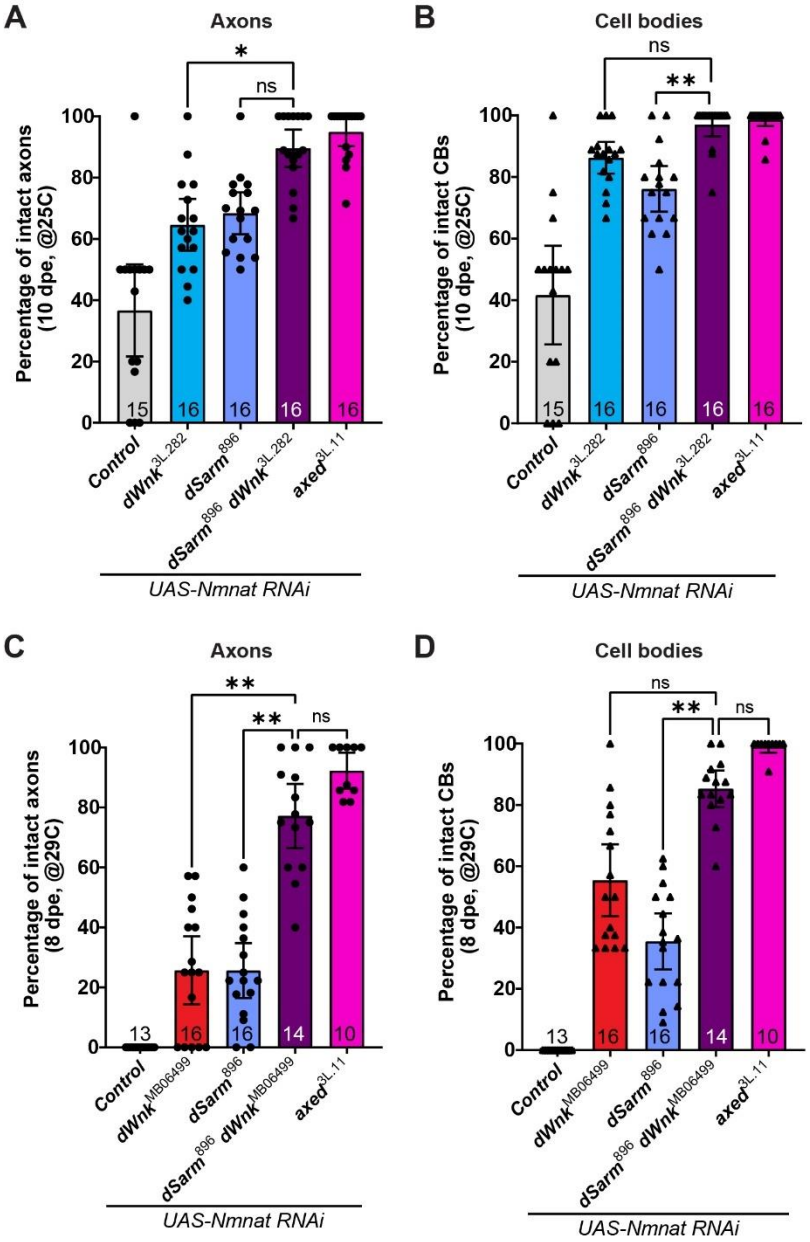
A
Axons
Percentage of intact axons (10 dpe, @25C)
*
ns
15
16
16
16
16
Control
dWnk3L.282
dSarm896
dSarm896 dWnk3L.282
axed3L.11
UAS-Nmnat RNAi
B
Cell bodies
Percentage of intact CBs (10 dpe, @25C)
ns
**
15
16
16
16
16
Control
dWnk3L.282
dSarm896
dSarm896 dWnk3L.282
axed3L.11
UAS-Nmnat RNAi
C
Axons
Percentage of intact axons (8 dpe, @29C)
**
**
ns
13
16
16
14
10
Control
dWnkMB06499
dSarm896
dSarm896 dWnkMB06499
axed3L.11
UAS-Nmnat RNAi
D
Cell bodies
Percentage of intact CBs (8 dpe, @29C)
ns
**
ns
13
16
16
14
10
Control
dWnkMB06499
dSarm896
dSarm896 dWnkMB06499
axed3L.11
UAS-Nmnat RNAi

Figure S4:

(A-B) The additive effect of the *dSarm*^{896}*,dWnk*$^{3L.282}$ double mutant compared to the single mutants and *axed*$^{3L.11}$ is evident in a standard *dNmnat KD* experiment (25°C). The results are plotted as mean ± 95% CI and analyzed using Kruskal-Wallis tests with post-hoc Dunn's multiple comparison test. All comparisons are listed in the Supplementary table 2. **(C-D)** *dWnk*^{MB06499} and *dSarm*^{896} partially protect axons **(C)** and neuronal cell bodies **(D)** from strong dNmnat depletion (29°C). *dSarm*^{896}*,dWnk*^{MB06499} double mutant axons **(C)** and cell bodies **(D)** are protected to the same extent as *axed KO*. The results are plotted as mean ± 95% CI and analyzed using Kruskal-Wallis tests with post-hoc Dunn's multiple comparison test. All comparisons are listed in the Supplementary table 2.

ACKNOWLEDGEMENTS

We thank all the lab members of Freeman lab for the suggestions and discussions on this work and manuscript writing. We thank Prof. Aylin Rodan in the University of Utah for sharing ncc69^{r1} and ncc69^{r2} flies. We thank Prof. Dietmar Schmucker in the University of Bonn, Germany for sharing dWnk^{F1183} and dWnk^{G1286} flies. We thank Dr. Li-Kroeger in Dr. Hugo Bellen lab in Baylor College of Medicine for sharing pBH vector.

References

Anselmo, A. N., Earnest, S., Chen, W., Juang, Y.-C., Kim, S. C., Zhao, Y., et al. (2006). WNK1 and OSR1 regulate the Na^+, K^+, $2Cl^-$ cotransporter in HeLa cells. *Proc. Natl. Acad. Sci. U.S.A.* 103, 10883–10888. doi: 10.1073/pnas.0604607103

Begum, G., Yuan, H., Kahle, K. T., Li, L., Wang, S., Shi, Y., et al. (2015). Inhibition of WNK3 Kinase Signaling Reduces Brain Damage and Accelerates Neurological Recovery After Stroke. *Stroke* 46, 1956–1965. doi: 10.1161/STROKEAHA.115.008939

Berger, J., Senti, K.-A., Senti, G., Newsome, T. P., Åsling, B., Dickson, B. J., et al. (2008). Systematic Identification of Genes that Regulate Neuronal Wiring in the Drosophila Visual System. *PLoS Genetics* 4, e1000085. doi: 10.1371/journal.pgen.1000085

Bhuiyan, M. I. H., Huang, H., Jiang, T., Taheri, T., Zhang, Z., and Sun, D. (2020). "WNK-SPAK/OSR1-CCC signaling in ischemic brain damage," in *Neuronal Chloride Transporters in Health and Disease*, (Elsevier), 431–461. doi: 10.1016/B978-0-12-815318-5.00017-0

Bloom, A. J., Mao, X., Strickland, A., Sasaki, Y., Milbrandt, J., and DiAntonio, A. (2022). Constitutively active SARM1 variants that induce neuropathy are enriched in ALS patients. *Mol Neurodegeneration* 17, 1. doi: 10.1186/s13024-021-00511-x

Bradshaw, D. V., Knutsen, A. K., Korotcov, A., Sullivan, G. M., Radomski, K. L., Dardzinski, B. J., et al. (2021). Genetic inactivation of SARM1 axon degeneration pathway improves outcome trajectory after experimental traumatic brain injury based on pathological, radiological, and functional measures. *acta neuropathol commun* 9, 89. doi: 10.1186/s40478-021-01193-8

Bratkowski, M., Xie, T., Thayer, D. A., Lad, S., Mathur, P., Yang, Y.-S., et al. (2020). Structural and Mechanistic Regulation of the Pro-degenerative NAD Hydrolase SARM1. *Cell Reports* 32, 107999. doi: 10.1016/j.celrep.2020.107999

Burke, R. E., and O'Malley, K. (2013). Axon degeneration in Parkinson's disease. *Experimental Neurology* 246, 72–83. doi: 10.1016/j.expneurol.2012.01.011

Chen, X., Kintner, D. B., Luo, J., Baba, A., Matsuda, T., and Sun, D. (2008). Endoplasmic reticulum Ca2+ dysregulation and endoplasmic reticulum stress following in vitro neuronal ischemia: role of Na+-K+-Cl- cotransporter. *Journal of Neurochemistry* 106, 1563–1576. doi: 10.1111/j.1471-4159.2008.05501.x

Chuang, C.-F. (2005). A Toll-interleukin 1 repeat protein at the synapse specifies asymmetric odorant receptor expression via ASK1 MAPKKK signaling. *Genes & Development* 19, 270–281. doi: 10.1101/gad.1276505

Coleman, M. P., and Höke, A. (2020). Programmed axon degeneration: from mouse to mechanism to medicine. *Nat Rev Neurosci* 21, 183–196. doi: 10.1038/s41583-020-0269-3

Di Stefano, M., Nascimento-Ferreira, I., Orsomando, G., Mori, V., Gilley, J., Brown, R., et al. (2015). A rise in NAD precursor nicotinamide mononucleotide (NMN) after injury promotes axon degeneration. *Cell Death & Differentiation* 22, 731–742. doi: 10.1038/cdd.2014.164

Dowd, B. F. X., and Forbush, B. (2003). PASK (Proline-Alanine-rich STE20-related Kinase), a Regulatory Kinase of the Na-K-Cl Cotransporter (NKCC1). *Journal of Biological Chemistry* 278, 27347–27353. doi: 10.1074/jbc.M301899200

Essuman, K., Summers, D. W., Sasaki, Y., Mao, X., DiAntonio, A., and Milbrandt, J. (2017). The SARM1 Toll/Interleukin-1 Receptor Domain Possesses Intrinsic NAD + Cleavage Activity that Promotes Pathological Axonal Degeneration. *Neuron* 93, 1334-1343.e5. doi: 10.1016/j.neuron.2017.02.022

Fang, Y., Soares, L., Teng, X., Geary, M., and Bonini, N. M. (2012). A Novel Drosophila Model of Nerve Injury Reveals an Essential Role of Nmnat in Maintaining Axonal Integrity. *Current Biology* 22, 590–595. doi: 10.1016/j.cub.2012.01.065

Figley, M. D., Gu, W., Nanson, J. D., Shi, Y., Sasaki, Y., Cunnea, K., et al. (2021). SARM1 is a metabolic sensor activated by an increased NMN/NAD+ ratio to trigger axon degeneration. *Neuron* 109, 1118-1136.e11. doi: 10.1016/j.neuron.2021.02.009

Geisler, S., Doan, R. A., Cheng, G. C., Cetinkaya-Fisgin, A., Huang, S. X., Höke, A., et al. (2019). Vincristine and bortezomib use distinct upstream mechanisms to activate a common SARM1-dependent axon degeneration program. *JCI Insight* 4. doi: 10.1172/jci.insight.129920

Geisler, S., Doan, R. A., Strickland, A., Huang, X., Milbrandt, J., and DiAntonio, A. (2016). Prevention of vincristine-induced peripheral neuropathy by genetic deletion of SARM1 in mice. *Brain* 139, 3092–3108. doi: 10.1093/brain/aww251

Gerdts, J., Brace, E. J., Sasaki, Y., DiAntonio, A., and Milbrandt, J. (2015). SARM1 activation triggers axon degeneration locally via NAD $^{+}$ destruction. *Science* 348, 453–457. doi: 10.1126/science.1258366

Gilley, J., and Coleman, M. P. (2010). Endogenous Nmnat2 Is an Essential Survival Factor for Maintenance of Healthy Axons. *PLoS Biology* 8, e1000300. doi: 10.1371/journal.pbio.1000300

Gilley, J., Jackson, O., Pipis, M., Estiar, M. A., Al-Chalabi, A., Danzi, M. C., et al. (2021). Enrichment of SARM1 alleles encoding variants with constitutively hyperactive NADase in patients with ALS and other motor nerve disorders. *eLife* 10, e70905. doi: 10.7554/eLife.70905

Gilley, J., Orsomando, G., Nascimento-Ferreira, I., and Coleman, M. P. (2015). Absence of SARM1 Rescues Development and Survival of NMNAT2-Deficient Axons. *Cell Reports* 10, 1974–1981. doi: 10.1016/j.celrep.2015.02.060

Goldsmith, E. J., and Rodan, A. R. (2023). Intracellular Ion Control of WNK Signaling. *Annu. Rev. Physiol.* 85, 383–406. doi: 10.1146/annurev-physiol-031522-080651

Henninger, N., Bouley, J., Sikoglu, E. M., An, J., Moore, C. M., King, J. A., et al. (2016). Attenuated traumatic axonal injury and improved functional outcome after traumatic brain injury in mice lacking *Sarm1*. *Brain* 139, 1094–1105. doi: 10.1093/brain/aww001

Hsu, J.-M., Kang, Y., Corty, M. M., Mathieson, D., Peters, O. M., and Freeman, M. R. (2020). Injury-Induced Inhibition of Bystander Neurons Requires dSarm and Signaling from Glia. *Neuron*, S0896627320308904. doi: 10.1016/j.neuron.2020.11.012

Izadifar, A., Courchet, J., Virga, D. M., Verreet, T., Hamilton, S., Ayaz, D., et al. (2021). Axon morphogenesis and maintenance require an evolutionary conserved safeguard function of Wnk kinases antagonizing Sarm and Axed. *Neuron* 109, 2864-2883.e8. doi: 10.1016/j.neuron.2021.07.006

Kahle, K. T., Khanna, A. R., Alper, S. L., Adragna, N. C., Lauf, P. K., Sun, D., et al. (2015). K-Cl cotransporters, cell volume homeostasis, and neurological disease. *Trends in Molecular Medicine* 21, 513–523. doi: 10.1016/j.molmed.2015.05.008

Kahle, K. T., Schmouth, J.-F., Lavastre, V., Latremoliere, A., Zhang, J., Andrews, N., et al. (2016). Inhibition of the kinase WNK1/HSN2 ameliorates neuropathic pain by restoring GABA inhibition. *Science Signaling* 9, ra32–ra32. doi: 10.1126/scisignal.aad0163

Kasahara, M., Menon, D. K., Salmond, C. H., Outtrim, J. G., Taylor Tavares, J. V., Carpenter, T. A., et al. (2010). Altered functional connectivity in the motor network after traumatic brain injury. *Neurology* 75, 168–176. doi: 10.1212/WNL.0b013e3181e7ca58

Kneynsberg, A., Combs, B., Christensen, K., Morfini, G., and Kanaan, N. M. (2017). Axonal Degeneration in Tauopathies: Disease Relevance and Underlying Mechanisms. *Front. Neurosci.* 11, 572. doi: 10.3389/fnins.2017.00572

Lafrenière, R. G., MacDonald, M. L. E., Dubé, M.-P., MacFarlane, J., O'Driscoll, M., Brais, B., et al. (2004). Identification of a Novel Gene (HSN2) Causing Hereditary Sensory and Autonomic Neuropathy Type II through the Study of Canadian Genetic Isolates. *The American Journal of Human Genetics* 74, 1064–1073. doi: 10.1086/420795

Leiserson, W. M., Harkins, E. W., and Keshishian, H. (2000). Fray, a Drosophila Serine/Threonine Kinase Homologous to Mammalian PASK, Is Required for Axonal Ensheathment. *Neuron* 28, 793–806. doi: 10.1016/S0896-6273(00)00154-9

Li-Kroeger, D., Kanca, O., Lee, P.-T., Cowan, S., Lee, M. T., Jaiswal, M., et al. (2018). An expanded toolkit for gene tagging based on MiMIC and scarless CRISPR tagging in Drosophila. *eLife* 7, e38709. doi: 10.7554/eLife.38709

Lunn, E. R., Perry, V. H., Brown, M. C., Rosen, H., and Gordon, S. (1989). Absence of Wallerian Degeneration does not Hinder Regeneration in Peripheral Nerve. *Eur J of Neuroscience* 1, 27–33. doi: 10.1111/j.1460-9568.1989.tb00771.x

Marion, C. M., McDaniel, D. P., and Armstrong, R. C. (2019). Sarm1 deletion reduces axon damage, demyelination, and white matter atrophy after experimental traumatic brain injury. *Experimental Neurology* 321, 113040. doi: 10.1016/j.expneurol.2019.113040

McCormick, J. A., Yang, C.-L., and Ellison, D. H. (2008). WNK Kinases and Renal Sodium Transport in Health and Disease: An Integrated View. *Hypertension* 51, 588–596. doi: 10.1161/HYPERTENSIONAHA.107.103788

Milde, S., Gilley, J., and Coleman, M. P. (2013). Subcellular Localization Determines the Stability and Axon Protective Capacity of Axon Survival Factor Nmnat2. *PLoS Biology* 11, e1001539. doi: 10.1371/journal.pbio.1001539

Moriguchi, T., Urushiyama, S., Hisamoto, N., Iemura, S., Uchida, S., Natsume, T., et al. (2005). WNK1 Regulates Phosphorylation of Cation-Chloride-coupled Cotransporters via the STE20-related Kinases, SPAK and OSR1. *Journal of Biological Chemistry* 280, 42685–42693. doi: 10.1074/jbc.M510042200

Neukomm, L. J., Burdett, T. C., Gonzalez, M. A., Züchner, S., and Freeman, M. R. (2014). Rapid in vivo forward genetic approach for identifying axon death genes in *Drosophila*. *Proceedings of the National Academy of Sciences* 111, 9965–9970. doi: 10.1073/pnas.1406230111

Neukomm, L. J., Burdett, T. C., Seeds, A. M., Hampel, S., Coutinho-Budd, J. C., Farley, J. E., et al. (2017). Axon Death Pathways Converge on Axundead to Promote Functional and Structural Axon Disassembly. *Neuron* 95, 78-91.e5. doi: 10.1016/j.neuron.2017.06.031

Osterloh, J. M., Yang, J., Rooney, T. M., Fox, A. N., Adalbert, R., Powell, E. H., et al. (2012). dSarm/Sarm1 Is Required for Activation of an Injury-Induced Axon Death Pathway. *Science* 337, 481–484. doi: 10.1126/science.1223899

Pathak, A., Stanley, E. M., Hickman, F. E., Wallace, N., Brewer, B., Li, D., et al. (2018). Retrograde Degenerative Signaling Mediated by the p75 Neurotrophin Receptor Requires p150Glued Deacetylation by Axonal HDAC1. *Developmental Cell* 46, 376-387.e7. doi: 10.1016/j.devcel.2018.07.001

Piala, A. T., Moon, T. M., Akella, R., He, H., Cobb, M. H., and Goldsmith, E. J. (2014). Chloride Sensing by WNK1 Involves Inhibition of Autophosphorylation. *Sci. Signal.* 7. doi: 10.1126/scisignal.2005050

Pleinis, J. M., Norrell, L., Akella, R., Humphreys, J. M., He, H., Sun, Q., et al. (2021). WNKs are potassium-sensitive kinases. *American Journal of Physiology-Cell Physiology*, ajpcell.00456.2020. doi: 10.1152/ajpcell.00456.2020

Ponce-Coria, J., San-Cristobal, P., Kahle, K. T., Vazquez, N., Pacheco-Alvarez, D., De Los Heros, P., et al. (2008). Regulation of NKCC2 by a chloride-sensing mechanism involving the WNK3 and SPAK kinases. *Proc. Natl. Acad. Sci. U.S.A.* 105, 8458–8463. doi: 10.1073/pnas.0802966105

Rahmani, B., Fekrmandi, F., Ahadi, K., Ahadi, T., Alavi, A., Ahmadiani, A., et al. (2018). A novel nonsense mutation in WNK1/HSN2 associated with sensory neuropathy and limb destruction in four siblings of a large Iranian pedigree. *BMC Neurol* 18, 195. doi: 10.1186/s12883-018-1201-6

Richardson, C., Rafiqi, F. H., Karlsson, H. K. R., Moleleki, N., Vandewalle, A., Campbell, D. G., et al. (2008). Activation of the thiazide-sensitive Na+-Cl– cotransporter by the WNK-regulated kinases SPAK and OSR1. *Journal of Cell Science* 121, 675–684. doi: 10.1242/jcs.025312

Rivière, J., Verlaan, D. J., Shekarabi, M., Lafrenière, R. G., Bénard, M., Der Kaloustian, V. M., et al. (2004). A mutation in the *HSN2* gene causes sensory neuropathy type II in a Lebanese family. *Annals of Neurology* 56, 572–575. doi: 10.1002/ana.20237

Russell, M. A., Ostafichuk, L., and Scanga, S. (1998). Lethal P- *lacZ* insertion lines expressed during pattern respecification in the imaginal discs of *Drosophila*. *Genome* 41, 7–13. doi: 10.1139/g97-099

Ryder, E., Ashburner, M., Bautista-Llacer, R., Drummond, J., Webster, J., Johnson, G., et al. (2007). The DrosDel Deletion Collection: A Drosophila Genomewide Chromosomal Deficiency Resource. *Genetics* 177, 615–629. doi: 10.1534/genetics.107.076216

Sasaki, Y., Kakita, H., Kubota, S., Sene, A., Lee, T. J., Ban, N., et al. (2020). SARM1 depletion rescues NMNAT1 dependent photoreceptor cell death and retinal degeneration. Neuroscience. doi: 10.1101/2020.04.30.069385

Sato, A., and Shibuya, H. (2013). WNK Signaling Is Involved in Neural Development via Lhx8/Awh Expression. *PLoS ONE* 8, e55301. doi: 10.1371/journal.pone.0055301

Sato-Yamada, Y., Strickland, A., Sasaki, Y., Bloom, J., DiAntonio, A., and Milbrandt, J. (2022). A SARM1-mitochondrial feedback loop drives neuropathogenesis in a Charcot-Marie-Tooth disease type 2A rat model. *Journal of Clinical Investigation* 132, e161566. doi: 10.1172/JCI161566

Schellinger, J. N., Sun, Q., Pleinis, J. M., An, S.-W., Hu, J., Mercenne, G., et al. (2022). Chloride oscillation in pacemaker neurons regulates circadian rhythms through a chloride-sensing WNK kinase signaling cascade. *Current Biology* 32, 1429-1438.e6. doi: 10.1016/j.cub.2022.03.017

Sengupta, S., Tu, S.-W., Wedin, K., Earnest, S., Stippec, S., Luby-Phelps, K., et al. (2012). Interactions with WNK (With No Lysine) Family Members Regulate Oxidative Stress Response 1 and Ion Co-transporter Activity. *Journal of Biological Chemistry* 287, 37868–37879. doi: 10.1074/jbc.M112.398750

Serysheva, E., Berhane, H., Grumolato, L., Demir, K., Balmer, S., Bodak, M., et al. (2013). Wnk kinases are positive regulators of canonical Wnt/β-catenin signalling. *EMBO reports* 14, 718–725. doi: 10.1038/embor.2013.88

Shekarabi, M., Girard, N., Rivière, J.-B., Dion, P., Houle, M., Toulouse, A., et al. (2008). Mutations in the nervous system–specific HSN2 exon of WNK1 cause hereditary sensory neuropathy type II. *Journal of Clinical Investigation*. doi: 10.1172/JCI34088

Shekarabi, M., Zhang, J., Khanna, A. R., Ellison, D. H., Delpire, E., and Kahle, K. T. (2017). WNK Kinase Signaling in Ion Homeostasis and Human Disease. *Cell Metabolism* 25, 285–299. doi: 10.1016/j.cmet.2017.01.007

Sporny, M., Guez-Haddad, J., Khazma, T., Yaron, A., Dessau, M., Mim, C., et al. (2020). The Structural Basis for SARM1 Inhibition, and Activation Under Energetic Stress. Biochemistry. doi: 10.1101/2020.08.05.238287

Spradling, A. C., Stern, D., Beaton, A., Rhem, E. J., Laverty, T., Mozden, N., et al. (1999). The Berkeley Drosophila Genome Project Gene Disruption Project: Single P-Element Insertions Mutating 25% of Vital Drosophila Genes. *Genetics* 153, 135–177. doi: 10.1093/genetics/153.1.135

Tang, X., Jaenisch, R., and Sur, M. (2021). The role of GABAergic signalling in neurodevelopmental disorders. *Nat Rev Neurosci* 22, 290–307. doi: 10.1038/s41583-021-00443-x

Turkiew, E., Falconer, D., Reed, N., and Höke, A. (2017). Deletion of Sarm1 gene is neuroprotective in two models of peripheral neuropathy. *J Peripheral Nervous Sys* 22, 162–171. doi: 10.1111/jns.12219

Veríssimo, F., and Jordan, P. (2001). WNK kinases, a novel protein kinase subfamily in multi-cellular organisms. *Oncogene* 20, 5562–5569. doi: 10.1038/sj.onc.1204726

Vitari, A. C., Deak, M., Morrice, N. A., and Alessi, D. R. (2005). The WNK1 and WNK4 protein kinases that are mutated in Gordon's hypertension syndrome phosphorylate and activate SPAK and OSR1 protein kinases. *Biochemical Journal* 391, 17–24. doi: 10.1042/BJ20051180

Wang, J., Zhai, Q., Chen, Y., Lin, E., Gu, W., McBurney, M. W., et al. (2005). A local mechanism mediates NAD-dependent protection of axon degeneration. *The Journal of Cell Biology* 170, 349–355. doi: 10.1083/jcb.200504028

Wilson, F. H., Disse-Nicodème, S., Choate, K. A., Ishikawa, K., Nelson-Williams, C., Desitter, I., et al. (2001). Human Hypertension Caused by Mutations in WNK Kinases. *Science* 293, 1107–1112. doi: 10.1126/science.1062844

Wu, J. S., and Luo, L. (2006). A protocol for mosaic analysis with a repressible cell marker (MARCM) in Drosophila. *Nature Protocols* 1, 2583–2589. doi: 10.1038/nprot.2006.320

Wu, Y., Schellinger, J. N., Huang, C.-L., and Rodan, A. R. (2014). Hypotonicity Stimulates Potassium Flux through the WNK-SPAK/OSR1 Kinase Cascade and the Ncc69 Sodium-Potassium-2-Chloride Cotransporter in the *Drosophila* Renal Tubule. *Journal of Biological Chemistry* 289, 26131–26142. doi: 10.1074/jbc.M114.577767

Xie, Y., Li, H., Luo, X., Li, H., Gao, Q., Zhang, L., et al. (2022). IBS 2.0: an upgraded illustrator for the visualization of biological sequences. *Nucleic Acids Research* 50, W420–W426. doi: 10.1093/nar/gkac373

Xu, B., English, J. M., Wilsbacher, J. L., Stippec, S., Goldsmith, E. J., and Cobb, M. H. (2000). WNK1, a Novel Mammalian Serine/Threonine Protein Kinase Lacking the Catalytic Lysine in Subdomain II. *Journal of Biological Chemistry* 275, 16795–16801. doi: 10.1074/jbc.275.22.16795

Xu, B., Min, X., Stippec, S., Lee, B.-H., Goldsmith, E. J., and Cobb, M. H. (2002). Regulation of WNK1 by an Autoinhibitory Domain and Autophosphorylation. *Journal of Biological Chemistry* 277, 48456–48462. doi: 10.1074/jbc.M207917200

Yarikipati, P., Jonusaite, S., Pleinis, J. M., Dominicci Cotto, C., Sanchez-Hernandez, D., Morrison, D. E., et al. (2023). Unanticipated domain requirements for Drosophila Wnk kinase in vivo. *PLoS Genet* 19, e1010975. doi: 10.1371/journal.pgen.1010975

Zagórska, A., Pozo-Guisado, E., Boudeau, J., Vitari, A. C., Rafiqi, F. H., Thastrup, J., et al. (2007). Regulation of activity and localization of the WNK1 protein kinase by hyperosmotic stress. *The Journal of Cell Biology* 176, 89–100. doi: 10.1083/jcb.200605093

Zhao, H., Nepomuceno, R., Gao, X., Foley, L. M., Wang, S., Begum, G., et al. (2017). Deletion of the WNK3-SPAK kinase complex in mice improves radiographic and clinical outcomes in malignant cerebral edema after ischemic stroke. *J Cereb Blood Flow Metab* 37, 550–563. doi: 10.1177/0271678X16631561

Zhao, Z. Y., Xie, X. J., Li, W. H., Liu, J., Chen, Z., Zhang, B., et al. (2019). A Cell-Permeant Mimetic of NMN Activates SARM1 to Produce Cyclic ADP-Ribose and Induce Non-apoptotic Cell Death. *iScience* 15, 452–466. doi: 10.1016/j.isci.2019.05.001